POLYMER FUNCTIONALIZATION OF SWNTS

POLYMER FUNCTIONALIZATION OF SINGLE-WALLED CARBON NANOTUBES THROUGH COVALENT METHODS

By

ZHAOLING YAO, B.Sc., M.Sc.

A Thesis
Submitted to the School of Graduate Studies
In Partial Fulfillment of the Requirements
For the Degree
Master of Science

McMaster University

MASTER OF SCIENCE (2004) McMaster University

(Chemistry) Hamilton, Ontario

TITLE: Functionalization of Single-Walled Carbon Nanotubes Through Covalent Methods

AUTHOR: Zhaoling Yao, B.Sc., M.Sc.

SUPERVISOR: Professor Alex Adronov

NUMBER OF PAGES: xiv, 81

Abstract

The discovery of nanotubes with unique mechanical, electrical, and thermal properties has led to their use in the development of the next generation of composite materials. However, their poor solubility and dispersion properties in any organic and aqueous solvents limits their potential applications.

In order to improve their solubility, single walled carbon nanotubes (SWNTs) were functionalized along their sidewalls with phenol groups using a 1,3-dipolar cycloaddition reaction. These phenols could be further derivatized with 2-bromoisobutyryl bromide, resulting in the attachment of atom transfer radical polymerization initiators to the sidewalls of the nanotubes. These initiators were found to be active in the polymerization of methyl methacrylate and t-butyl acrylate from the surface of the nanotubes. However, the polymerizations were not controlled, leading to the production of high molecular weight polymeric grafts with relatively large polydispersities. The resulting polymer carrying nanotubes were analyzed by IR, Raman spectroscopy, solid state NMR, DSC, TEM and AFM. The nanotubes functionalized with poly(methyl methacrylate) were found to be insoluble in organic solvents, such as THF and CH_2Cl_2. However, the dispersion property of SWNTs in polymer matrix was improved dramatically.

Another momoner t-butyl acrylate (t-BuA) was also polymerized using the same macroinitiators. It was found that the SWNTs functionalized with t-BuA

were soluble in a variety of organic solvents. The t-butyl groups of these appended polymers could also be removed to produce nanotubes functionalized with poly (acrylic acid), resulting in nanocomposites that are soluble in aqueous solutions.

In addition, polystyrene (PS) which was prepared by stable free radical polymerization, was used to functionalize SWNTs through the radical coupling reaction. IR, NMR, TEM and AFM confirmed that this polystyrene was covalently bonded to the SWNTs. It was also found that the resulting PS-SWNTs composites were quite soluble in organic solvents, such as THF and CH_2Cl_2.

Acknowledgement

I would like to thank my supervisor, Dr. Alex Adronov, who always kept an eye on the progress of my work and my English, and took effort in reading and providing me with valuable comments on earlier versions of this thesis. I also want to thank Dr. Harald D.H. Stöver and Dr. K. Saravanamuttu for being my committee members and their cheerful assistance during my study period.

I would like to thank Yuanqin Liu, Greg Bahun, Hai Wang and Matt Parrott for many discussions about chemistry and for providing me friendly help in work and life during the last three years.

I feel a deep sense of gratitude for my parents who taught me the good things that really matter in life. I am very grateful for my husband, Houzhi Pan, for his understanding, love and support during my study. One of the best experiences that we lived through in this period was the birth of our son, Daniel Pan, who provided an additional and joyful dimension to our life mission.

This work was supported by grants from the Natural Science and Engineering Research Council of Canada (NSERC), the Canada Foundation for Innovation, the Ontario Innovation Trust, as well as McMaster University. Additionally, I would like to thank Frank Gibbs for thermal analysis data, G. Timmins and Bernard Pointner for the Raman spectroscopy data, Nadi Braidy and

Prof. G. A. Botton for TEM data, Prof. Gillian R. Goward and Lindsey Cahill for solid-state NMR data, as well as Andy Duft for AFM measurement.

TABLE OF CONTENTS

Page

List of Schemes

List of Figures

List of Tables

Chapter 1 Introduction

1.1 Single walled carbon nanotubes (SWNTs) and their properties

In addition to graphite, diamond and fullerenes, a fourth carbon family member, carbon nanotubes (Figure 1-1) were discovered by Sumio Iijima in 1991[1]. The carbon nanotubes reported by Iijima are multi-walled carbon nanotubes (MWNTs). Two years later, another category of carbon nanotubes called single-walled carbon nanotubes (SWNTs) was also found by Iijima and coworkers.[2] Both MWNTs and SWNTs are composed of sp^2 hybridized carbon atoms. SWNTs can be thought of as a single graphene sheet rolled up into a cylinder with a typical diameter on the order of 1-2 nm. The length of the well-defined cylindrical structures of SWNTs vary from microns to multiple centimeters.[3]

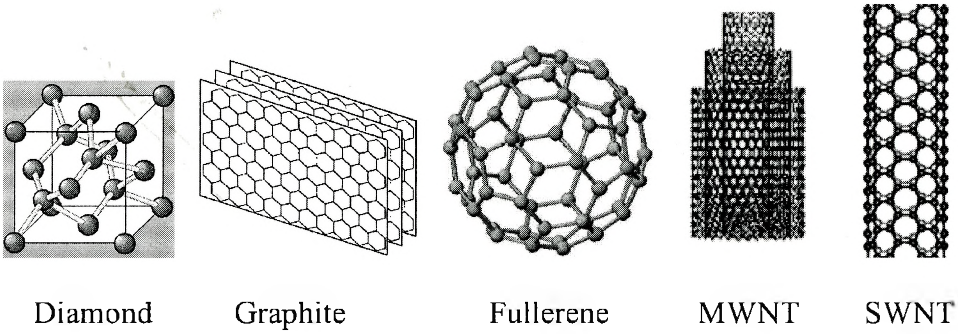

Figure 1-1. Schematic structures of carbon family.

Depending on their diameter and chirality, SWNTs have different conductivity properties and they can be either one-dimensional metals or semiconductors. The structure of a SWNT is uniquely characterized by the roll-up vector, $\mathbf{R} = m\mathbf{a}_1 + n\mathbf{a}_2$, where $\mathbf{a}_1$ and $\mathbf{a}_2$ are the graphene primitive vectors and *m, n* are integers (Figure 1-2).[4] These integers represents lattice points (m, n) and can be used to index different types of nanotubes. Among the large number of possible **R** vectors, there are two inequivalent high-symmetry directions. These are termed as "zigzag" and "armchair" and are designated by (m, 0) and (m, m), respectively. Basically, all armchair tubes are metallic. One out of three zigzag and chiral tubes show a small bandgap due to the curvature of the graphene sheet, while all other tubes are semi-conducting with a bandgap that scales approximately with the inverse of the tube radius.

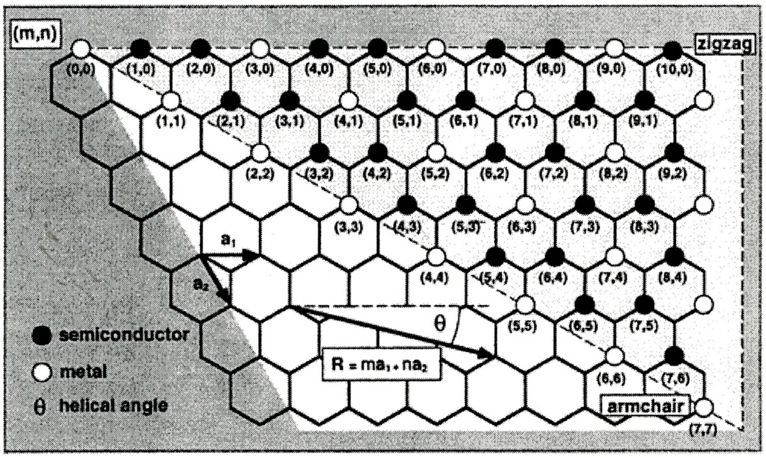

Figure 1-2. Indexing scheme that shows the folding procedure to create nanotube cylinders from planar graphene sheets. All the (*m*, *m*) type nanotubes form armchair tubes and all (m, 0) tubes are zigzag tubes. (Reprinted from ref. 4)

In addition to their conductivity properties, the mechanical strength (Young's modulus) of SWNTs is five times higher than that of steel.[5,6] It has been reported recently that they exhibit high mechanical resilience,[7,8] which allows them to be bent without breaking.

Essentially, SWNTs are insoluble in most organic and aqueous solvents because they are entangled together through π- π stacking to form bundles. The insolubility of SWNTs has hindered most of their potential applications. Therefore, increasing the solubility of SWNTs has attracted significant attention.

1.2 Approaches to synthesize SWNTs

Arc discharge,[1,9,10] laser ablation[11] and chemical vapour deposition [12-14] are the main methods used for carbon nanotube synthesis. Arc discharge and laser ablation use solid state carbon precursors as carbon sources and involve carbon vaporization at high temperature. Chemical vapour deposition (CVD) employs hydrocarbon gases as carbon sources and metal catalyst particles to serve as "seeds" needed for nanotube growth. A relatively lower temperature is needed for this approach. One particular CVD method named the HiPco (High Pressure Carbon monoxide disproportionation)[15] process, which was developed by Smalley's group, uses carbon monoxide at high pressure as a feedstock. This is a gas-phase catalytic process where the catalyst (iron-metal clusters) is formed from the pyrolysis of iron pentacarbonyl, $Fe(CO)_5$, at 800°C.[15] Carbon monoxide disproportionates to form elemental carbon and CO_2, which occurs catalytically on the surface of the iron particles, upon which SWNTs nucleate and grow. Compared to other methods, the HiPco process is a scalable synthetic technique and it can produce approximately one kilogram of SWNTs per day.

1.3 Potential applications of SWNTs

The potential utility of single walled carbon nanotubes (SWNTs) in a variety of technologically important applications, such as molecular wires and electronics,[16,17] sensors,[18] high-strength fibers,[19] and field emission[20] is now well established.

Due to their high tensile strength and high mechanical resilience, incorporation of SWNTs into plastics can potentially provide structural materials with significantly increased modulus and strength.[21-24] For instance, Biercuk and co-workers observed a monotonic increase of resistance to indentation (Vickers hardness) by 3.5 times with a 2% SWNTs loading in epoxy resin and a doubled thermal conductivity with 1% SWNTs.[23] Cadek and coworkers [24] reported that they carried out tensile tests on free-standing composite films of poly(vinyl alcohol) and carbon nanotubes for different nanotube loading levels and observed significant increases in Young's modulus by up to a factor of 2 in all cases. They showed that reinforcement scales linearly with the total nanotube surface area in the films.

The unique electronic properties of nanotubes make them qualified for use as quantum wires. The conductivity properties of this class of nanoscale materials have attracted a great deal of investigation, which has immensely expanded their scope of applicability. Based on a single semiconducting SWNT, the Dekker group has built the first single-molecule field-effect transistor (FET), an essential component for next-generation computing.[25] Field emission devices are one of the more promising nanotube applications being developed by industry and academia, which utilize SWNTs as field emission electron sources.[26,27] The work of Dekker,[28-30] Lieber,[31-34] and Avouris[16] has also demonstrated that SWNTs can not only be utilized as the semiconducting channels in functional field effect transistors, but that they can outperform comparable Si-based devices. In addition, Dai and co-workers have shown that SWNTs can act as chemical sensors, where exposure to specific gases, including NH_3, NO_2, and H_2, alters nanotube conductivity by up to three orders of magnitude within several seconds of exposure.[35,36] The mechanical robustness and conductivity of SWNTs make it possible to use SWNTs as Atomic Force Microscopy (AFM) tips,[37,38] which are now commercially available from Daiken Chemical Company, Ltd. SWNTs have also been utilized in photovoltaic devices by Kymakis and co-workers.[39-41] They developed poly(3-octylthiophene) (P3OT) based photovoltaic devices that, when doped with SWNTs, have an increased photocurrent by more than two orders of magnitude.

1.4 Chemical Functionalization of SWNTs

Although significant progress in the nanotube field has been made, several major limitations have yet to be overcome and currently preclude the widespread commercial utility of carbon nanotubes. The inherent insolubility of SWNTs in most organic and aqueous solvents is a limiting factor that must be overcome if SWNTs are to be incorporated in useful products for a wide range of applications. In order to realize the potential applications of carbon nanotubes, a number of research groups have focused on the chemical functionalization of SWNTs with various organic, inorganic, and organometallic structures using both covalent and non-covalent approaches. Many of these studies focus on improving the solubility properties of nanotubes. The primary success was achieved by functionalizing carboxylic acid groups, formed at the ends and defect sites of SWNTs during oxidative purification/shortening, through amidation with alkyl amines such as octadecyl amine. This approach has been extended to the attachment of organometallic complexes, including Vaska's complex[42] and Wilkinson's catalyst,[43] inorganic nanocrystals such as CdSe[44,45] and Au,[46] DNA[47,48] and various other biological molecules,[49-51] dendrons,[52] and polymers[53]. Another strategy for SWNT functionalization employs sidewall reactions such as fluorination with elemental fluorine,[54] 1,3-dipolar cycloaddition,[55,56] electrochemical reduction of diazonium salts,[57] the Bingel reaction (cyclopropanation)[58] and direct addition of nitrenes, carbenes, and radicals to the unsaturated π-system of the nanotubes.[59] These side-wall functionalization strategies have been used to result in much higher degrees of functionalization than previous approaches allowing chemists to control the properties of these nano-scale materials.

Recently selective chemical reactions on SWNTs have been reported by Wong[60] and Liu's[61] groups. Wong and coworkers[60] carried out a reaction in which SWNTs reacted with osmium tetroxide (OsO_4) in solution upon exposure to O_2 and UV irradiation at 254 nm. As a result, OsO_4 species were reduced to form OsO_2, which was preferentially covalently bonded to the sidewall of metallic SWNTs. Liu and coworkers[61] demonstrated a simple method for *in situ* fabrication of high-performance, excluding semiconducting SWNT network FETs by selectively eliminating metallic nanotubes in the devices using a diazonium reaction. Based on these differential reactivities of SWNTs, the modification of electronic, optical, and mechanical properties of SWNTs in a controllable manner is promising, which is essential for applications such as the development of nanotube-based electrodes as well as advances in molecular electronics [60].

Additionally, a number of recent reports have concentrated on supramolecular functionalization of SWNTs, especially with polymeric structures. The aromatic sidewalls of nanotubes provide the possibility for π-stacking interactions with conjugated polymers[62-67] as well as polycyclic aromatic hydrocarbons. The use of substituted pyrene molecules for surface attachment of a number of functionalities has also been implemented, where the appended structure has been used to attach proteins,[68] polymerization initiators,[69] or aqueous solubilizing groups[70] in a non-covalent fashion.

Among all of these chemical modification methods, it has been identified that one of the most promising approaches to increase the solubility of SWNTs is the covalent functionalization of carbon nanotubes with polymers. A number of reports have demonstrated the feasibility of attaching amine- and alcohol-functionalized polymeric structures to the surface of SWNTs through amidation and esterification with the carboxylic acid groups at the ends and defect sites of shortened SWNTs. Using these reactions, SWNT conjugates with various polymers, including poly(ethylene imine),[71] poly(styrene),[72] poly(ethylene oxide),[73] poly(vinyl carbazole),[74] and poly(vinyl alcohol)[75] have been prepared.

1.5 Living free radical polymerizations

Control over polymer architecture, molecular weight and polydispersity in a facile manner has been one of the important goals in polymer chemistry. Until recently, ionic polymerizations including cationic and anionic polymerizations have been used to gain well-defined polymer architecture including controlled molecular weight and narrow polydispersity. However, ionic polymerization methods require a demanding experimental setup and is limited to certain types of monomers. With the ability of providing the control of living polymerizations without the demanding experimental conditions, living radical polymerizations have attracted much research interest over the last decade.[76-86] It offers the opportunity to introduce high degrees of control over physical and chemical properties of polymers through the manipulation of molecular weight, polydispersity, chemical composition and polymer architecture. Nitroxide-mediated Stable Free Radical Polymerization (SFRP),[76-79] Atom Transfer Radical Polymerization (ATRP),[80-83] and Reversible Addition Fragmentation Transfer Polymerization (RAFT)[84-86] are three of the most common techniques for living radical polymerizations.

1.5.1 Atom transfer radical polymerization (ATRP)

A successful ATRP is accomplished through fast initiation and rapid, reversible deactivation, where all the chains grow in a relatively slow and uniform manner. A general mechanism for ATRP is shown in Scheme 1-1.[82] The reaction is catalyzed by a transition metal complex (M_t^n-Y/Ligand, where M_t^n is a transition metal and Y is a halogen atom) through a reversible redox process. It is a one-electron oxidation with simultaneous abstraction of a halogen atom, X, affording a dormant species, R-X. The addition of the vinyl monomers to the active radicals to form polymer chains is similar to a conventional radical polymerization. Termination reactions also occur in ATRP, mainly through radical coupling and disproportionation. However, in a well-controlled ATRP, less than a few percent of the polymer chains would undergo termination reactions. The generated oxidized metal complexes, X-M_t^{n+1}-Y, act as the persistent radicals to reduce the stationary concentration of growing radicals and thereby minimize the contribution of termination.

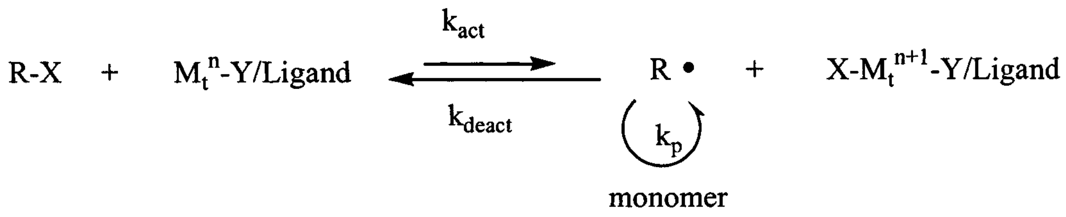

Scheme 1-1. General mechanism for ATRP.

Typical monomers for ATRP include styrenes, (meth)acrylates, (meth)acrylamides, and acrylonitrile, where the substituents can stabilize the propagating radicals. Alkyl bromides and chlorides are typically used as the initiators, as they have been found to promote rapid initiation and excellent molecular weight control. A variety of transition metal complexes have been utilized as ATRP catalysts, including Copper (Cu), Ruthenium (Ru), Iron (Fe) and Rhenium (Re). So far, the majority of the work has been reported using the copper based systems. ATRP can be carried out in bulk, in solution, or in a heterogeneous system (e.g., emulsion, suspension). Various solvents, such as benzene, toluene, anisole, diphenyl ether, dimethyl formamide (DMF), alcohol, water, and many others, have been used for different monomers. The polymerization temperature depends mostly on the monomer, the catalyst, and the desired molecular weight.

1.5.2 Stable Free Radical Polymerization (SFRP)

In SFRP, nitroxides such as 2,2,5,5-tetramethyl-3-(1-phenylethoxy)-4-chloromethylphenyl-3-azahexane,[79] compound **1**, homolytically dissociate (Scheme 1-2) at 125°C to form carbon-centered free radicals (initiating radicals) and oxygen-centered free radicals, 2,2,5,5-tetramethyl-4-phenyl-3-azahexane-3-nitroxide, compound **2** (persistent radicals). The oxygen-centered free radicals are essentially stable and will not initiate polymerization or couple to one another, but can couple to existing radicals and act as radical capping agents, thereby decreasing the concentration of free radicals in solution and diminishing termination steps.

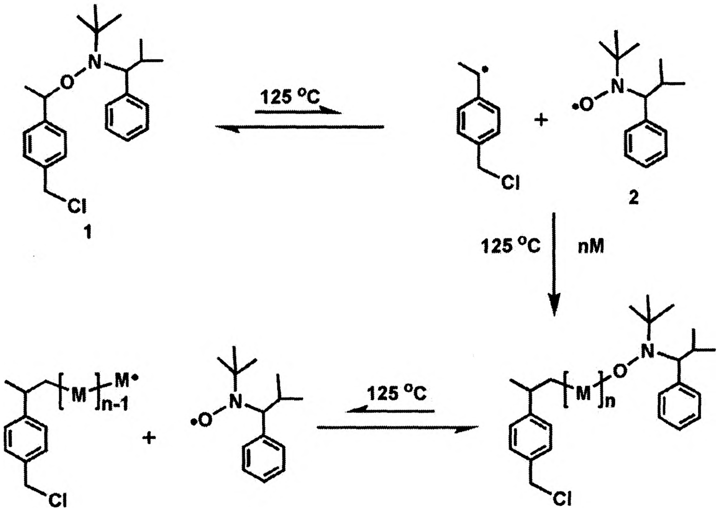

Scheme 1-2. General mechanism of SFRP using 2,2,5,5-tetramethyl- 3-(1-phenylethoxy)-4-chloromethylphenyl-3-azahexane as initiator.

Some additives, such as acetic anhydride and stable free nitroxide radicals (the radical to which the corresponding initiator will thermally decompose) are normally used to obtain a faster polymerization rate or narrower polydispersity.[87] The role of acetic anhydride is to stabilize the nitroxide radicals by acylation of the alkoxyamine nitrogen and thus increase the polymerization rate.[87] Some members in the family of nitroxides[79] permit the polymerization of a wide variety of monomers: styrenics, acrylates, acrylamides, 1,3-dienes and acrylonitrile, among which, styrenics are the easiest monomer family to be polymerized under SFRP in a living/controlled manner.

Recently it has been shown that radical coupling chemistry also could be applied to polymer functionalization of carbon nanotubes. Shaffer and Koziol demonstrated that polystyrene molecules were attached to the surface of oxidized multi-wall carbon nanotubes using an *in-situ* radical polymerization reaction.[88] Another similar work was carried out by Resasco and co-workers in which SWNT-filled polystyrene and styrene-isoprene composites were prepared by miniemulsion polymerization.[89] Both of these approaches showed a high polymer grafting efficiency and high solubility of polymer-nanotube composites in toluene. However, the molecular weight of attached polymers was not controlled due to the free radical polymerization process.

1.6 "Grafting from" and "grafting to" approaches

In terms of tethering polymer chains to the SWNTs, "grafting from" and "grafting to" methods can be utilized by using the above mentioned living radical polymerizations. In the "grafting from" method (Scheme 1-3), initiator molecules are first chemically bonded to SWNTs and polymers are then formed during a subsequent polymerization reaction. Several steps are needed to obtain the desired polymer functionalized SWNT materials. Also the reactions prior to polymerization are difficult to carry out due to the insolubility of SWNTs. In the 'grafting to' method (Scheme 1- 4), the polymers are first synthesized and then coupled to the SWNTs in a subsequent step utilizing specific functional groups that are reactive towards the nanotubes. In this approach, it is easier to control the molecular weight, polydispersity and the structure of the attached polymers. However, once the surface of SWNTs is covered with polymer molecules, this layer acts as a diffusion barrier for further chains that try to reach the surface, thus the graft density is lower than that of the "grafting from" approach.

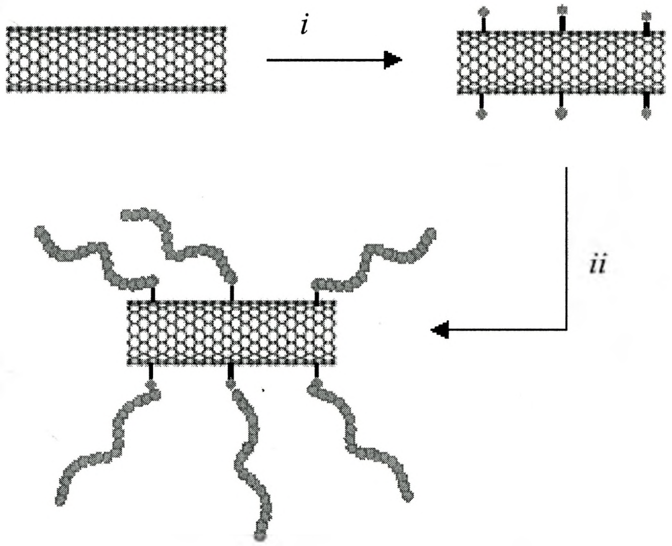

Scheme 1-3. General scheme for "Grafting from" approach.

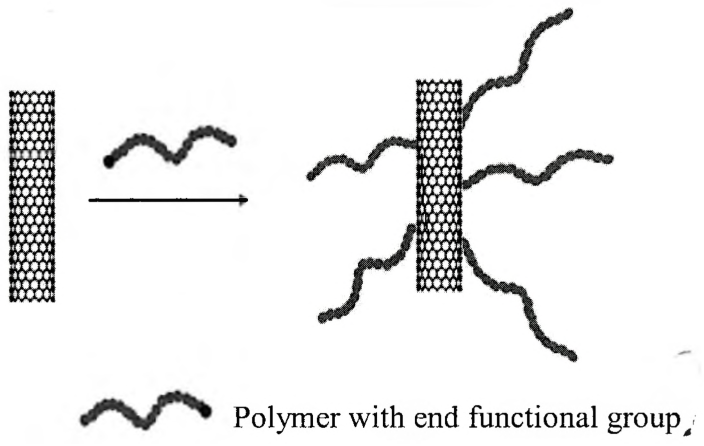

Scheme 1-4. General scheme for "Grafting to" approach.

1.7 Characterization of functionalized SWNTs

The characterization of functionalized SWNTs is critical to determine if the functionalization reactions succeeded or failed. The characterization of products represents a constant problem in nanotube chemistry because so far no technique alone provides adequate characterization of chemically modified SWNTs. However various techniques have been successfully used together to characterize pristine and functionalized SWNTs, such as Raman, Transmission Electron Microscopy (TEM), Scanning Electron Microscopy (SEM), Atomic Force Microscopy (AFM), Differential Scanning Calorimetry (DSC), Thermal Gravimetric Analysis (TGA), UV-vis, as well as solution and solid state NMR.

1.7.1 Raman Spectroscopy

Raman spectroscopy offers a great deal of information concerning the functionalization of SWNTs,[90] especially in cases of significant sidewall modification (Figure 1-3).[57] Raman spectra of SWNTs exhibit two characteristic modes: the diameter dependent radial breathing mode (ca. 230 cm^{-1}), and the higher frequency tangential mode (ca. 1590 cm^{-1}). The position of the radial breathing mode is directly proportional to tube diameter and is therefore extremely useful in characterizing nanotube structure and properties. A third mode, the so-called disorder mode (ca. 1295 cm^{-1}) is diagnostic of disruptions in the hexagonal framework of the SWNTs due to the defects or functionality. The relative intensity of this mode can then provide direct evidence of covalent modifications. For example, Tour and coworkers[57] showed that reaction of SWNTs with diazonium salts resulted in highly functionalized SWNTs. Here, the relative intensity of the disorder mode after functionalization (Figure 1-3b) is much greater than the pristine tubes (Figure 1-3a). This is an expected result of the introduction of covalently bound molecules to the nanotube framework, wherein significant amounts of the sp^2 carbons have been converted to sp^3 hybridization.

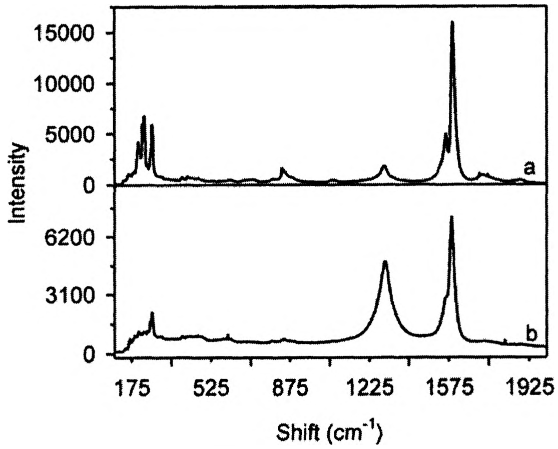

Figure 1-3. Raman scattering spectra pure (a) and derivatized samples (b) (Reprinted from ref. 57).

1.7.2 Thermal Gravimetric Analysis (TGA)

Thermal gravimetric analysis (TGA) gives useful insight into functionalized SWNTs, because it has been shown that most functionalizing moieties are thermally labile, while the SWNTs are stable to very high temperatures (~1000°C). By analyzing the results of TGA, the functionalization degree of SWNTs can be estimated.

1.7.3 Microscopy techniques

SEM, TEM, Scanning Tunneling Microscopy (STM) and AFM are powerful techniques that offer much insight about the structures and morphologies of SWNTs and their functionalized derivatives.[91,92] TEM, SEM and AFM images of pristine SWNTs are shown in Figure 1-4 A, B and C, respectively. Although the resolution of these techniques is generally not sufficient to directly observe moieties attached by chemical modification, perturbation of SWNT electronic structure can be probed, as well as functionalization effects on dispersion and exfoliation of ropes.

STM allows atomically resolved imaging of surface structures. It has been used to record atomically resolved images of pure SWNTs and of structural defects contained in them.[93-96] Individual functional groups on sidewall functionalized SWNTs have also been imaged with STM (Figure 1-4 D)[97].

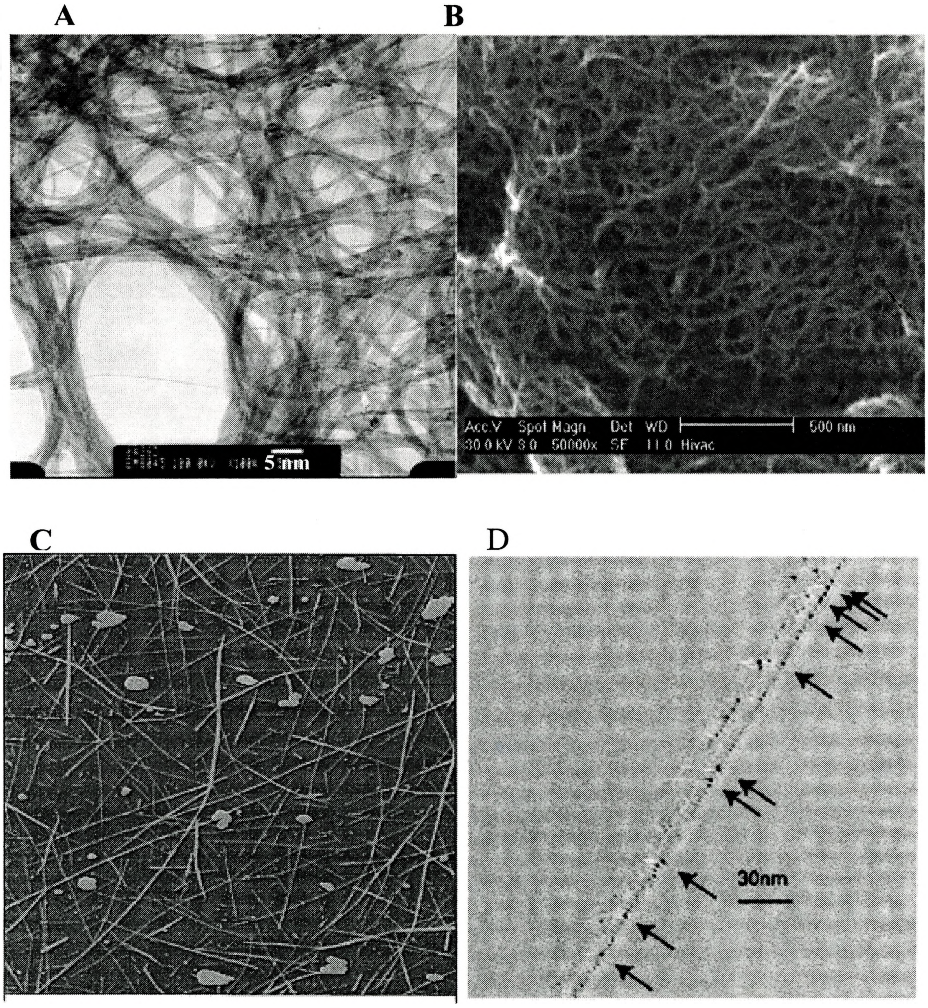

Figure 1-4. TEM (A) (Reprinted from ref. 91), SEM (B) (Reprinted from ref. 91), AFM (C) (Reprinted from ref. 92), and STM (D) (Reprinted from ref. 97) images of SWNTs.

1.7.4 UV-vis Absorption

Figure 1-5 shows the UV absorption spectrum of the pristine SWNTs in 1,2-dichlorobenzene.[98] The inset plot shows absorbance at 500 nm of SWNT solutions with different concentrations. The slope is analogous to the extinction coefficient of Beer's Law. This value can be used to determine the concentration of functionalized or pure SWNT samples.

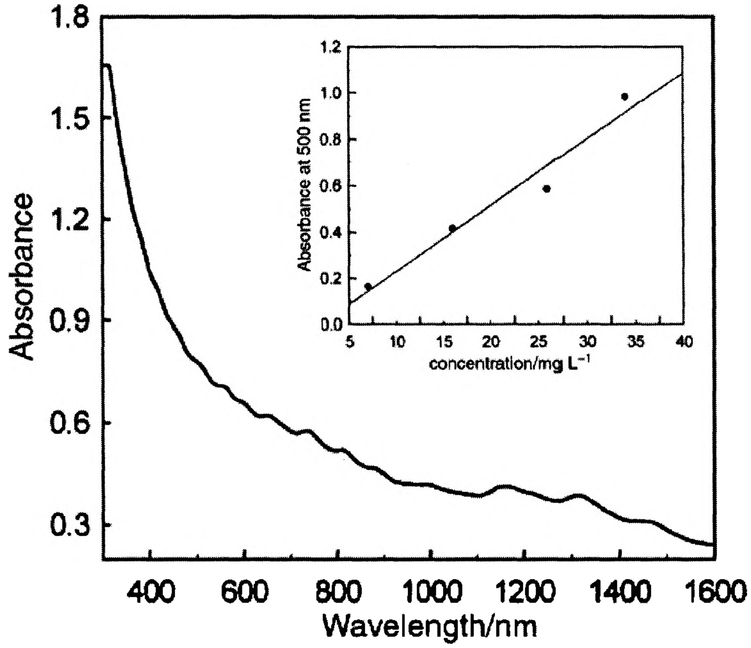

Figure 1-5. UV-vis absorption spectrum of the SWNT material at a concentration of 27 mg L^{-1} in 1,2-dichlorobenzene. Inset: Optical density at 500 nm of the SWNT material in 1,2-dichlorobenzene at different concentrations. The straight line is a linear-least-squares fit to the data; slope = 0.0286 (Reprinted from ref. 98).

Chapter 2 Objectives

The aim of this research project was to increase the solubility and processibility of SWNTs by functionalizing them with various polymers. From chapter 1 we know that there are two approaches to attach polymer chains to SWNTs, i.e. "grafting from" and "grafting to". Both methods are utilized in our research.

Also, we postulated shortened SWNTs were easier to dissolve after functionalization with polymers. Therefore, the as-received SWNTs were shortened under harsh acid condition (H_2SO_4/HNO_3) before functionalization with polymers.

2.1 Polymer Functionalization of SWNTs via ATRP

In this approach, SWNT based macroinitiators were first made by a 2-step process, where a 1,3-dipolar cycloaddition reaction was followed by an esterification reaction. The 1,3-dipolar cycloaddition reaction on the surface of SWNTs was performed using octanal and 4-hydroxyphenyl glycine to produce phenol-functionalized SWNTs that could be further derivatized with an ATRP initiator, 2-bromoisobutyryl bromide. We chose methyl methacrylate (MMA) as the monomer in this ATRP procedure because the reaction can be carried out at room temperature at a reasonable rate. In order to make water soluble SWNT nanocomposites, another monomer, t-butyl acrylate (t-BuA), was also polymerized by using the same macroinitiators because the t-butyl groups can be easily converted to acid groups.

Scheme 2-1 illustrates the "grafting from" approach utilized in this work, in which shortened SWNTs were first modified by a linker through the 1,3-dipolar reaction and then ATRP initiator was attached via an esterification reaction. In the presence of this macroinitiator, methyl methacrylate and t-butyl acrylate were polymerized.

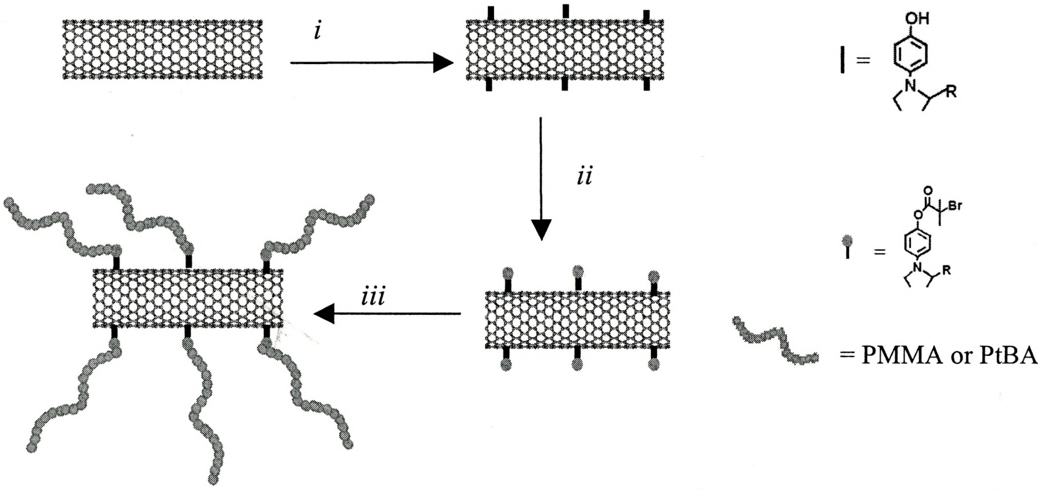

Scheme 2-1. "Grafting from" approach using ATRP. *i*: 1,3-dipolar cycloaddition reaction using octanal and 4-hydroxyphenyl glycine; *ii*: An esterification reaction between –OH groups on the surface of SWNTs and 2-bromoisobutyryl bromide; *iii*: Polymerization of MMA or t-BuA using the SWNTs based macroinitiators.

2.2 Functionalization of SWNTs via a radical coupling reaction

Polymer functionalization of carbon nanotubes with radicals has been reported recently by Shaffer and Koziol.[88] This approach, however, results in poor control over molecular weight and polydispersity in synthesized polymers due to the nature of free radical polymerizations. To prepare carbon nanotubes that are functionalized with polymers with well-defined structures, living free radical polymerizations may be feasible since they work in a controlled manner and, more importantly, radicals can be readily produced during or after polymerization reactions.

Following this idea, it was proposed that SFRP could be utilized to functionalize SWNTs with polymers via the radical coupling reaction at elevated temperature, resulting in SWNTs that exhibit improved solubility. Nitroxide-terminated polystyrene can be prepared by "living" free-radical polymerization utilizing one of the universal alkoxyamine unimolecular initiators recently introduced by Hawker and co-workers.[79]

"Grafting to" approaches were attempted to functionalize shortened SWNTs. Preformed polymers with well controlled molecular weights and low polydispersities were covalently attached to SWNTs. In this project polystyrene **2** was prepared first by SFRP. At 125°C the nitroxide-terminated polystyrene can generate two kinds of radicals, stable nitroxide radicals and carbon centered radicals which were believed to be trapped by SWNTs through a radical coupling reaction to give PS-SWNT nanocomposites **4** (Scheme 2-2). The resulting well-defined polymer-nanotube conjugates exhibited high solubility in various organic solvents, such as THF, CH_2Cl_2 and $CHCl_3$.

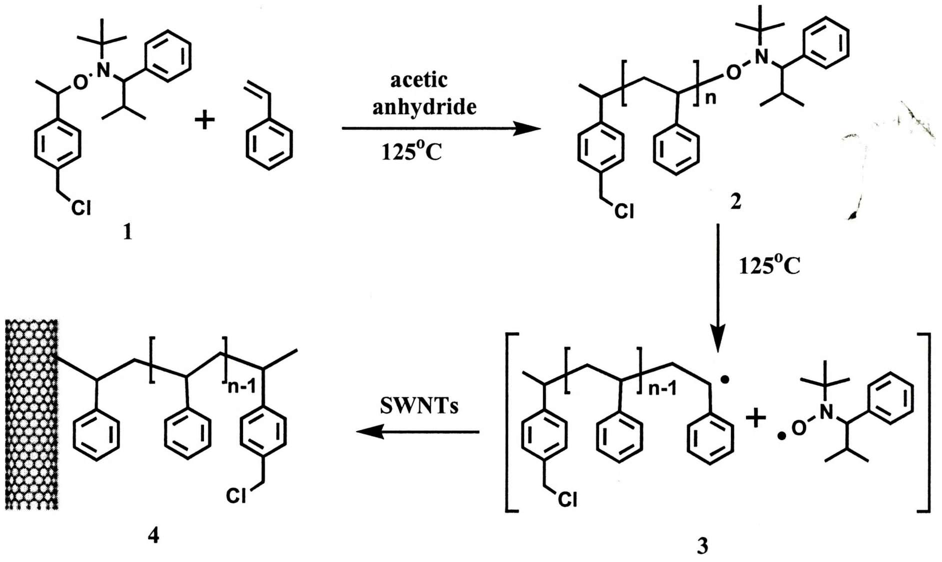

Scheme 2-2. "Grafting to" approach to make PS-SWNTs composites.

Chapter 3 Polymerization of MMA from SWNTs

3.1 Overview

The carbon nanotube starting materials we utilized were purchased from Carbon Nanotechnologies, Inc. (Houston, TX), and were already purified. However, there were still some Fe nanoparticles that remained in the nanotubes. It was postulated that this may affect the polymerization later, thus the as-received SWNTs were further purified (see below). At the same time, SWNTs were shortened during the purification procedure, which also met our primary goal because we postulated that functionalization of shortened nanotubes would have a higher probability of producing soluble structures.

Upon obtaining shortened SWNTs, macroinitiators were made first and then the monomer of interest was polymerized using the macroinitiators. Atom transfer radical polymerization (ATRP) of methyl methacrylate (MMA) is known to be a facile process that occurs efficiently in solution due to the relative ease of activation of the capped radical species and the favorable ATRP equilibrium constant.[82] For these reasons, we initially chose MMA as the monomer.

3.2 Shortening and purification of SWNTs

The average length of pristine SWNTs were approximately 1.5 to 2 μm, and 1 to 1.5 nm in diameter. During the purification process, they were shortened to various average lengths by varying the shortening time. The shortening procedure we followed was a slightly modified version of the procedure published by Smalley and co-workers.[99] Our only modification to this procedure was a reduced sonication time in the 3:1 mixture of H_2SO_4:HNO_3 from 24 hrs to approximately 3 hrs. In our hands, and with our ultrasonicator (Branson Ultrasonics B1510), it was found that sonication for more than 6 hrs leaves no trace of carbon nanotubes, as determined by atomic force microscopy (AFM). This may be due to the difference in sonicating power between the Branson (70 Watt) sonicator we used, and the Cole Parmer (20 Watt) sonicator used by Smalley. The shortened SWNTs were isolated by filtration through a polycarbonate membrane having a pore size of 100 nm. The products were characterized by AFM and FTIR.

Figure 3-1 shows AFM images of carbon nanotubes at different sonication time periods. It is clear that a substantial shortening is occurring after only a short period of sonication, with a length reduction of approximately 40-50% after each hour.

It should be noted that the purchased nanotube samples are polydisperse in terms of length, and, therefore, a variety of different lengths can be observed in each AFM image. Length analysis of 100 different nanotubes after 2 h of shortening indicated an average length of 334 nm.

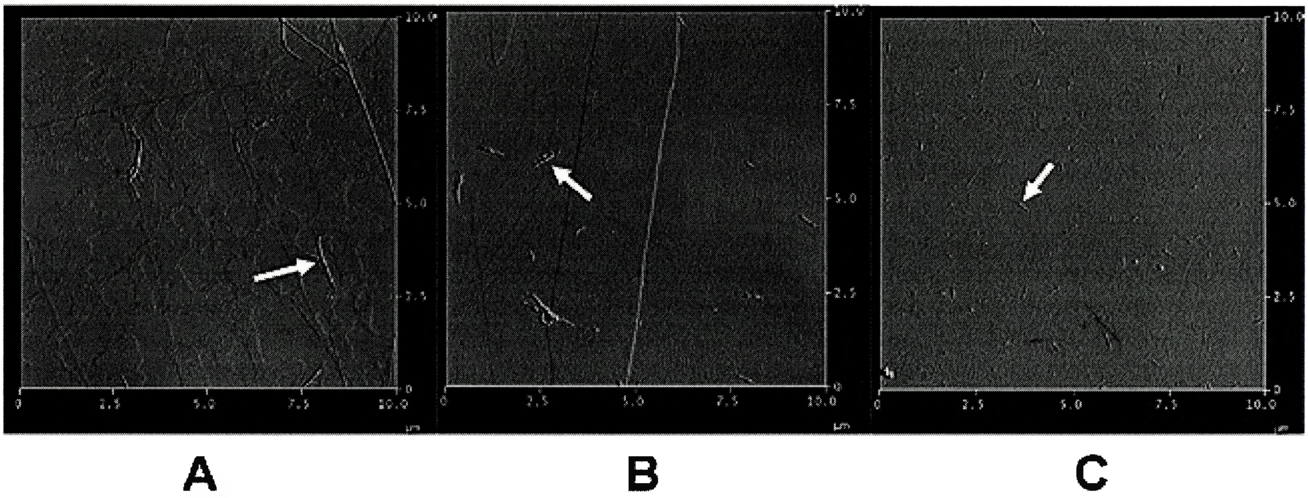

Figure 3-1. AFM images of the shortening process for SWNTs. A) As-received SWNTs; B) SWNTs after sonication for 1 h; C) SWNTs after sonication for 2 h.

The product of this procedure was characterized by IR spectroscopy (Figure 3-2) and exhibited the expected C=O stretch at 1741 cm-1 arising from the carboxylic acid groups introduced as a result of the shortening process. The large IR band observed at ca. 3400 cm-1 and the weak one at 1627 cm-1 are attributed to the asymmetrical stretching and scissoring vibrations, respectively, due to traces of water in the KBr pellet used for the analysis. The trace water could not be removed even with extensive drying of the KBr at elevated temperatures and prolonged purging of the instrument with a stream of nitrogen gas.

Figure 3-3 illustrates the Raman spectra of the shortened, unfunctionalized nanotubes. The characteristic absorptions of the nanotubes are clearly observable at ca. 260 and 1590 cm^{-1}, corresponding to the radial breathing modes (RBM) and the tangential G band, respectively. In addition, the broad disorder band at 1300 cm^{-1} indicates the presence of sp^3 hybridized C atoms, which are known to occur at defect sites in the nanotube structure.

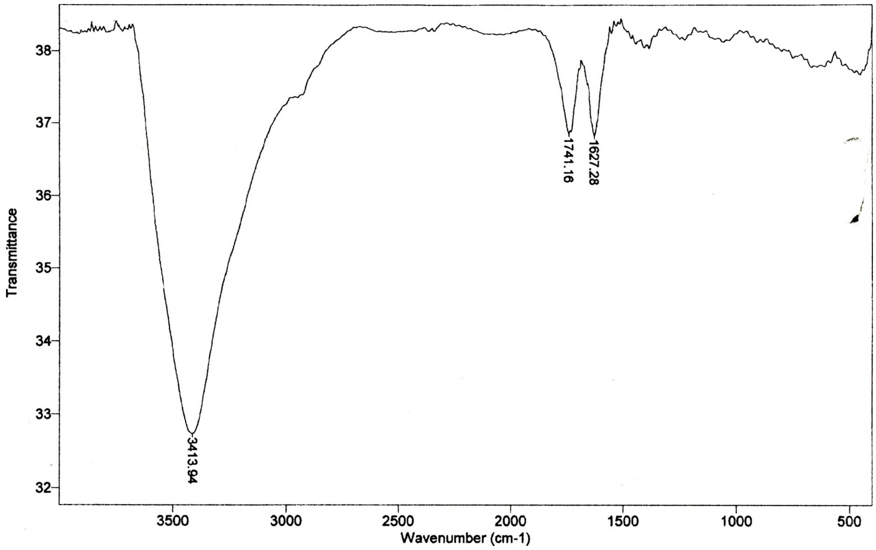

Figure 3-2. IR spectrum for the shortened SWNTs.

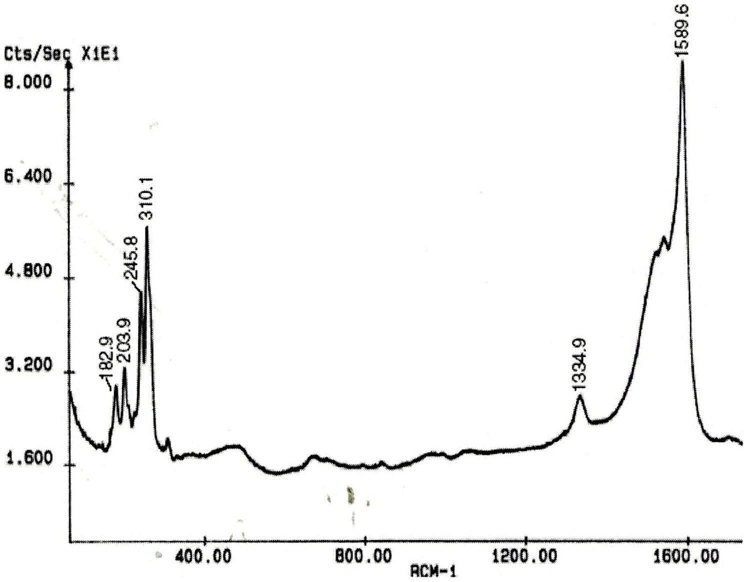

Figure 3-3. Raman spectrum for the shortened SWNTs.

3.3 Functionalization of SWNTs with ATRP initiators

In order to attach atom transfer radical polymerization initiators,[82] such as alkyl halides, especially alkyl bromides, to form SWNT based ATRP macroinitiaotors, we first functionalized the sidewalls of our shortened nanotubes using the 1,3-dipolar cycloaddition reaction (Scheme 3-1).

Addition of 4-hydroxyphenyl glycine and octyl aldehyde to a suspension of shortened SWNTs in DMF, followed by heating at 130°C for five days resulted in the incorporation of phenol-functionalized pyrrolidine rings on the surface of the SWNTs. This was evidenced by the appearance of a clear C-H stretch at ca. 2900 cm^{-1} and an increase in the aromatic C-C stretch at 1634 cm^{-1} in the IR spectrum (Figure 3-4). The surface phenol functionalities could then be treated with 2-bromoisobutyryl bromide to introduce the initiating species on the sidewalls of the tubes (Scheme 3-1). This functionalization reaction was again

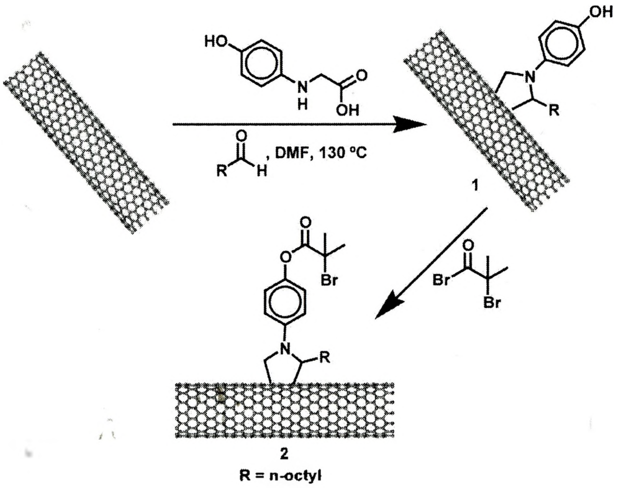

Scheme 3-1. Functionalization of SWNTs with ATRP initiator.

followed by IR spectroscopy to monitor the appearance of C-H stretches (ca. 2900 cm^{-1}) from the alkyl portions of the attached initiators, and the appearance of a strong C=O stretch (ca. 1730 cm^{-1}) arising from the ester linkages (Figure 3-5).

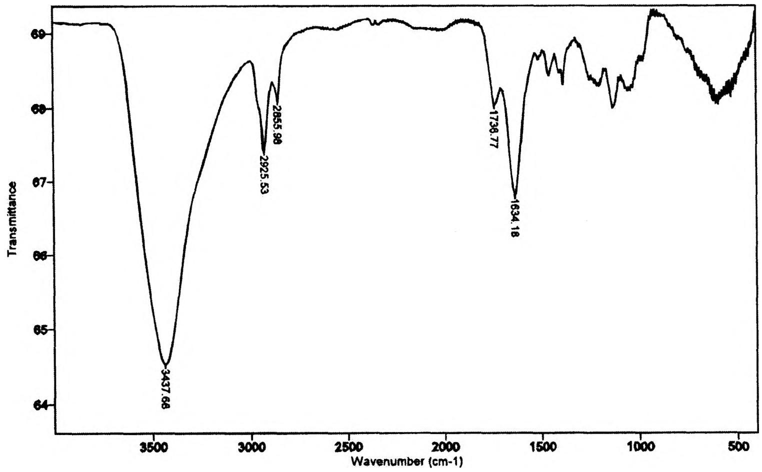

Figure 3-4. IR spectrum of phenol-functionalized SWNTs.

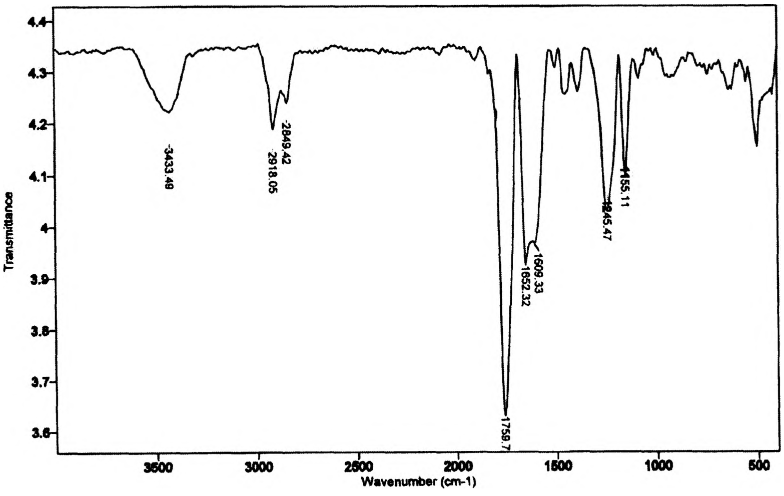

Figure 3-5. IR spectrum of initiator-functionalized SWNTs.

3.4 Polymerization of MMA using SWNT macroinitiators.

Polymerization of MMA using the SWNT macroinitiators (Scheme 3-2) was implemented under various conditions (Table 3-1). In order to successfully carry out this polymerization, it was necessary to choose a solvent in which the functionalized SWNTs could be well dispersed. It was also necessary to perform this reaction at a lower temperature to minimize any spontaneous thermal polymerization and to prevent cleavage of the phenolic ester linkage between the initiating site and the nanotube.

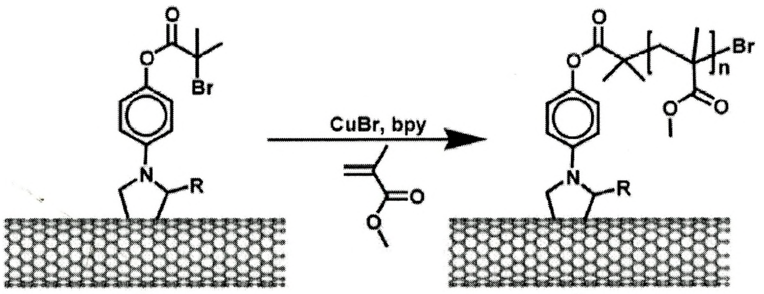

2
R = n-octyl

3

Scheme 3-2. Polymerization of SWNTs using the ATRP macroinitiator.

We performed several experiments in which polymerization conditions were varied, and they are summarized in Table 3-1. From these experiments, we found that an 8:3 mixture of DMF: H_2O as the solvent, and CuBr/2,2'-dipyridyl (bpy) as the catalyst/ligand system allowed for adequate dispersion of the macroinitiators. In addition, polymerization of acrylate monomers using this solvent and catalyst system has been demonstrated to be effective at room temperature with relatively short reaction times.[100] In a typical polymerization, one flask was charged with 4 mg of macroinitiator (**2**), 11 mL of a DMF/H_2O mixture (8:3 v/v) as the solvent, and 3 mL of MMA. This heterogeneous mixture was degassed by bubbling with a stream of N_2 for 30 min. A separate flask was charged with CuBr (40 mg) and bipyridine (175 mg) and was kept under an Ar atmosphere. Upon completion of the bubbling, the macroinitiator-containing suspension was transferred to the catalyst-containing flask via cannula, and this reaction flask was sealed. The resulting suspension was stirred at room temperature for various periods of time, ranging from 1 to 48 h. The polymerizations were then worked up by diluting with THF and filtering though a 200 nm pore Teflon (Millipore) membrane. The residue was washed with THF, CH_2Cl_2, and MeOH (approximately 200 mL of each) to remove excess monomer, the catalyst complex, and any unattached polymer that may have been formed in the polymerization process. Upon drying the residue under vacuum, a gray powder was isolated. This isolated product was then analyzed by IR and Raman spectroscopy, Differential Scanning Calorimetry, ^1H MAS NMR as well as AFM and TEM to determine its composition.

Table 3-1. Polymerization conditions and the corresponding results

Solvent systems	**ligands**	**Temp.**	**Observations**
Bulk (MMA only)	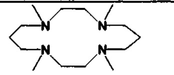	R.T.	SWNTs macroinitiators not dispersed well, no mass increase
CH_2Cl_2	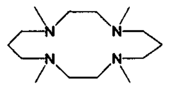	R.T.	SWNTs macroinitiators not dispersed well, no mass increase
DMF/H_2O (8:3 v/v)	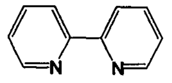	R.T.	SWNTs macroinitiators not disperse well, mass of product increased-polymer formed

3.4.1 Characterization of the polymerized SWNTs

Figure 3-6 illustrates the IR spectrum of a SWNT sample after 48 hours of polymerization, clearly indicating the expected carbonyl stretch at ~1730 cm^{-1} and C-H stretches at ~2950 cm^{-1} arising from the nanotube-attached PMMA in the sample. The presence of carbon nanotubes in this residue was confirmed through the use of Raman spectroscopy, which resulted in a spectrum exhibiting the characteristic tangential band (ca. 1590 cm^{-1}) and radial breathing modes (200-300 cm^{-1}) of carbon nanotubes, as well as a disorder band (1338 cm^{-1}) that corresponds to the presence of sp^3 hybridized carbon atoms, formed as a result of sidewall functionalization (Figure 3-7). This combination of IR and Raman data indicates that both the nanotube and polymer components are present in the sample and cannot be separated by washing with good solvents for the polymer. It should be noted that in a control experiment, where nanotubes were mixed with pre-formed PMMA, filtration and washing using the same protocol as outlined above resulted in complete removal of the free polymer from the nanotube residue, as indicated by an absence of IR stretches at ~1730 cm^{-1} and ~2900 cm^{-1} upon analysis of the residue.

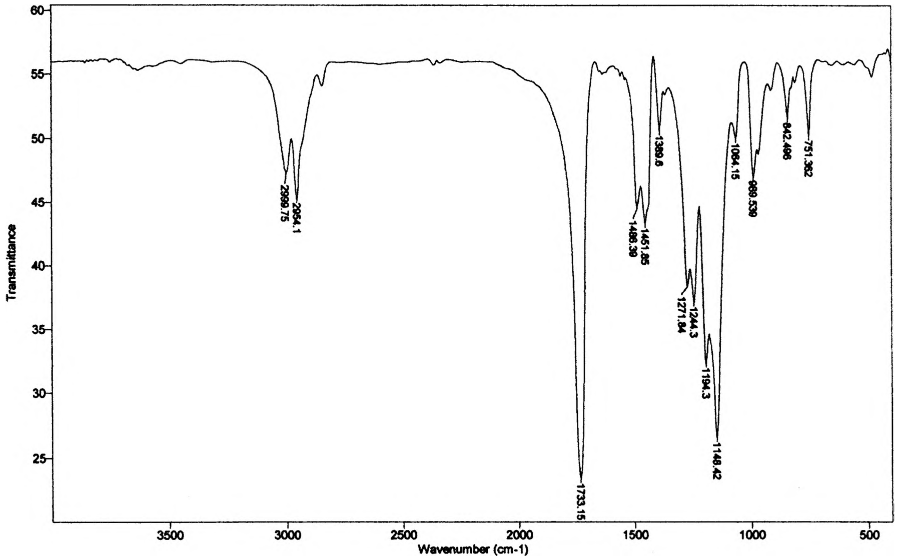

Figure 3-6. IR spectrum of SWNT-PMMA polymerized product.

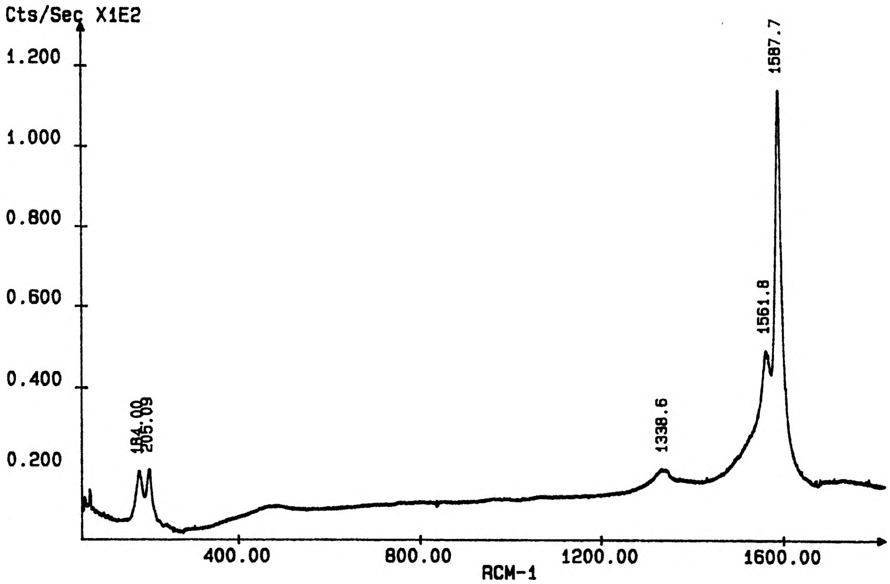

Figure 3-7. Raman spectrum of SWNT-PMMA polymerized product.

Due to the low solubility of PMMA functionalized SWNTs, solution NMR can not be used to characterize the composites. Whereas, the obtained solid state ^{1}H MAS NMR spectra[97] confirmed the effectiveness of each functionalization step. The purified, shortened SWNTs (Figure 3-8a) show only a single, very weak signal at 6.9 ppm, attributed to the protons associated with the carboxylic acid groups introduced at the ends and defects of the shortened nanotubes. The ^{1}H spectrum of **1**, Figure 3-8b, exhibits an aromatic resonance at 6.4 ppm, attributed to the four protons on the phenol ring, as well as a strong resonance at 0.5 ppm, assigned to the protons in the aliphatic heptyl chain. The comparison to the initiator-functionalized nanotubes, **2**, in Figure 3-8c, shows a marked broadening of the aliphatic resonance. Figure 3-8d shows the ^{1}H MAS spectrum of the PMMA-functionalized SWNTs, **3**, in which the dominant resonances belong to the two types of aliphatic protons in the polymer backbone and side chains, namely, the methylene protons at 0.9 ppm and the methoxy protons at 3.6 ppm. A very weak signal from the phenol groups of the initial functionalization is still visible at 7 ppm; however, the dominant PMMA signals indicate the relatively high molecular weight of the polymers grown from the comparatively small number of initiator sites.

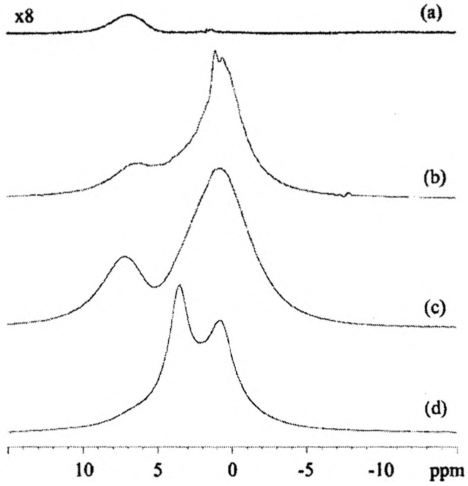

Figure 3-8. ^{1}H MAS SSNMR spectra acquired under 30 kHz magic-angle spinning: (a) purified, shortened nanotubes; (b) phenol nanotubes (**1**); (c) initiator nanotubes (**2**); and (d) PMMA-functionalized nanotubes (**3**).

Figure 3-9 illustrates the differential scanning calorimetry traces for bulk PMMA (Mn = 8972, PDI = 1.16) and PMMA prepared using the SWNT macroinitiators. It was observed that the glass transition temperature (Tg) of the polymer increased from 122°C in the bulk, to ca. 128°C when attached to the nanotubes. It has previously been shown that constraint of polystyrene chains resulting from their attachment to silica surfaces results in an increase in the Tg.[101] The same phenomenon may be occurring in this case, where attachment of the polymer chains to the nanotube surface imposes constraints over their mobility, resulting in the observed 6°C increase in Tg. In addition, polymers cleaved from the nanotubes under basic conditions were analyzed by DSC and exhibited a Tg of 121°C, again indicating that the elevated Tg was the result of nanotube attachment.

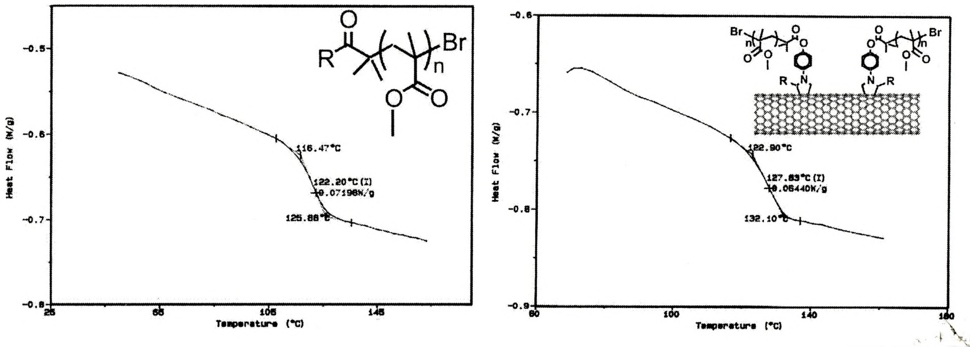

Figure 3-9. DSC traces for PMMA (A) and PMMA polymerized from the surface of SWNTs (B).

Further evidence for the formation of nanotube-polymer composites can be ascertained from microscopy studies. Figure 3-10 illustrates atomic force microscopy images of initiator functionalized (A) and polymer functionalized (B) SWNTs. The measured height profiles of representative initiator-functionalized tubes (*i* and *ii* in Figure 3-10 A) revealed that they were bundles, ranging in height between 5 and 15 nm, depending on the structure. This indicates that sidewall functionalization of the tubes with relatively small structures does not lead to the dissociation of nanotube bundles. Upon polymerization of MMA, it is clear that large, globular structures became associated with the carbon nanotubes. It is postulated that these structures correspond to nanotube-attached PMMA. The height profiles of the larger globular structures indicate heights ranging from 20 to 40 nm. Smaller polymer associated structures can also be observed. Interestingly, in Figure 3-10 B, a portion of a single SWNT can be seen spanning the distance between two polymerized areas, indicating that either initiator functionalization is not homogeneously spread over the entire length of the

SWNTs, or that some initiator sites are inhibited during the polymerization. Additionally, the height of this nanotube structure was measured to be on the order of 0.9 nm, indicating that it is a single tube, rather than a bundle of tubes. It is possible that, during polymerization, at least some of the SWNTs initially present in bundles are separated into individual tubes, presumably due to steric repulsion caused by the growing polymer chains.

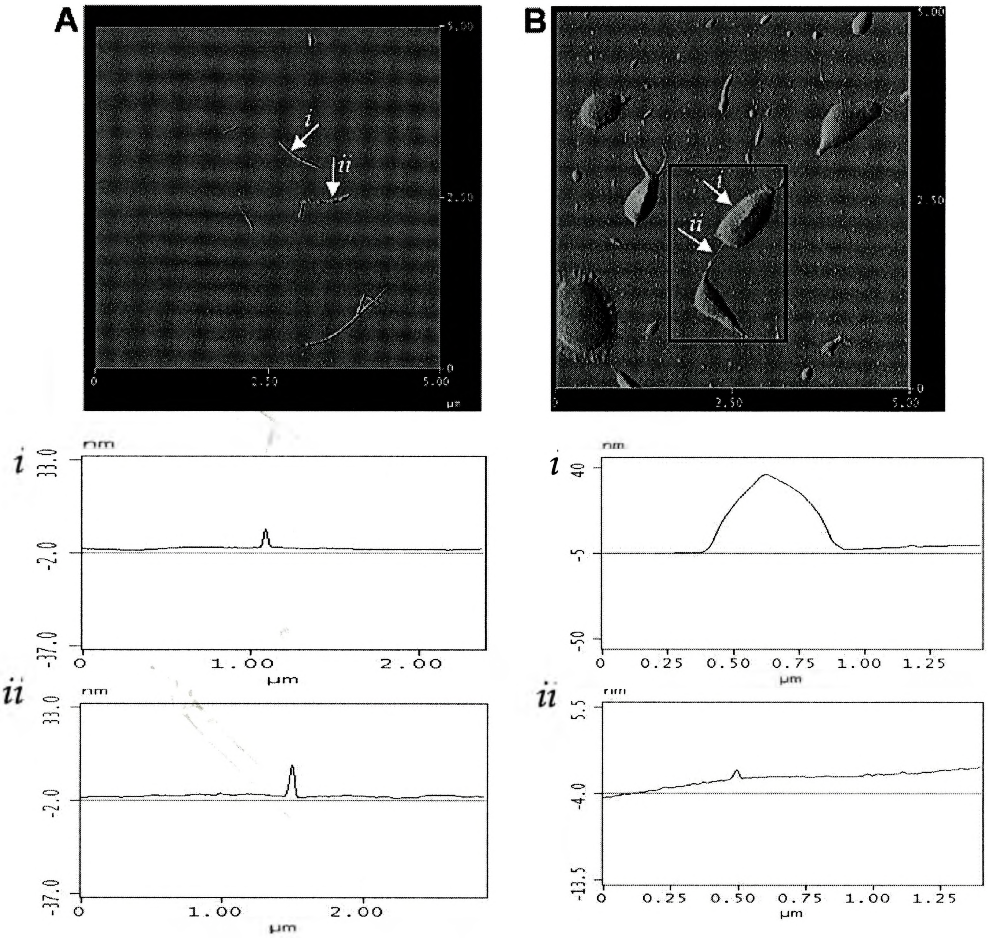

Figure 3-10. AFM images and height profiles of initiator functionalized carbon nanotubes before (A) and after (B) polymerization of MMA. Arrows indicate the location at which the cross-sectional height profiles were obtained.

Polymer coated SWNTs were also observed by transmission electron microscopy (TEM). Micrographs obtained by dispersing suspensions of the polymerized nanotubes onto a holey carbon grid clearly indicated the presence of nanotubes surrounded by regions of amorphous carbon, presumably corresponding to the polymer portion of the sample. Figure 3-11 illustrates an interconnected network of polymer sheathed SWNTs. In this image, several regions can be seen in which bare nanotubes span the distance between two areas of polymer. These nanotube "bridges" are composed either of individual tubes or of very small bundles, made up of two or three tubes. Again, this image provides some evidence that larger nanotube bundles are separated through the polymerization process, likely as a result of steric repulsion between growing polymer chains. It is interesting to note the interconnected nature of the polymer/SWNT strands, which may indicate that some degree of polymer tangling is occurring in these samples. It is possible that the polymer chains become crosslinked to a small extent as a result of radical coupling during the nanotube initiated ATRP process.

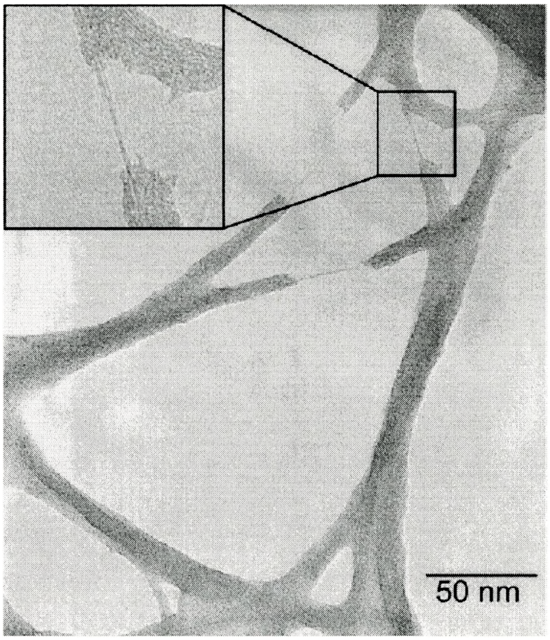

Figure 3-11. TEM micrograph of SWNT-PMMA nanocomposites.

3.4.2 Livingness of the ATRP process

In order to gain insight into whether or not the nanotube-initiated MMA polymerization process is a controlled/living polymerization, a study was performed in which the sample mass increase and the polymer molecular weight (MW) (Table 3-2) were correlated to the polymerization time. The mass increase of the samples after a specific polymerization interval was measured gravimetrically after filtration, washing with excess solvent, and thorough drying of the samples in vacuo. The molecular weight of the polymers was measured by GPC after cleaving the phenolic ester bond that links the initiator to the nanotube using excess $NaHCO_3$ in a mixture of $MeOH/CH_2Cl_2$ (2:7 v/v).[102] After cleavage, the polymer was isolated by first diluting the reaction mixture with THF and then passing the solution through a plug of silica gel with THF as the eluent. Any SWNTs present in the sample were easily removed by this procedure, allowing the isolation of pure polymer samples. It was found that the mass of the nanotube sample increased with time in a nearly linear fashion, but the polymer molecular weight did not follow this trend (Figure 3-12). In fact, extremely high MWs in excess of 300,000 g/mol were observed even after relatively short polymerization times (2 h). In addition, the polydispersity index (PDI) of the recovered polymer chains was consistently greater than 1.6. These results indicate that, as the polymerization time increases, more nanotube-bound initiators are able to initiate polymerization, resulting in the observed mass increase. However, based on the molecular weight and polydispersity data, it is clear that the polymerization process is not controlled. All attempts to chain extending the grafted polymers resulted in no mass increase, again indicating that the polymerizations were not living and had terminated irreversibly.

Table 3-2. Molecular weight data for polymers cleaved from SWNT Surfaces.

Reaction time	Mass increase (mg)	Mn (cleaved polymers) (g/mol)	PDI(cleaved polymers)
1	11.7	---	---
2	34	349,000	1.74
4	41	675,000	2.50
6	44	1,071,000	1.93
8	81	1,088,000	1.65
10	83	658,000	1.66
12	123	1,219,000	1.78

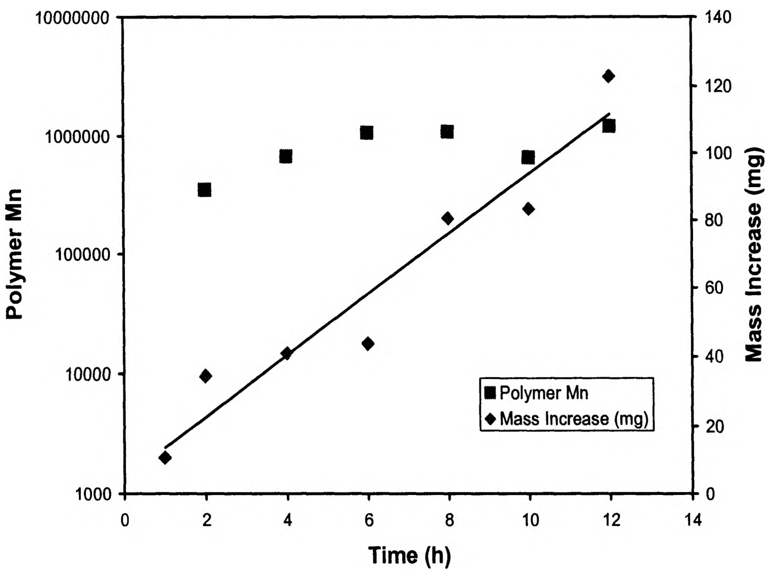

Figure 3-12. Evolution of the mass increase of the nanotube-PMMA composites and polymer molecular weight as a function of polymerization time.

A recent report has demonstrated that ATRP using surface-bound initiators results in uncontrolled, very rapid polymerization due to an extremely low concentration of the deactivating $CuBr_2$ species in solution.[103] It was demonstrated that addition of either sacrificial initiator or the $CuBr_2$ deactivator to the reaction mixture resulted in recovery of control over the polymerization from silicon substrates.[103,104] We postulated that similar approaches might help to control the SWNT-initiated polymerizations and produce narrow polydispersity chains attached to the nanotubes. However, our attempts to add sacrificial initiators to the nanotube-initiated polymerizations resulted in the exclusive formation of free polymer in solution, with no observable mass increase in the recovered nanotube samples. Clearly, the extremely low number of nanotube-attached initiating sites could not compete with the unattached initiators in the reaction mixture. Additionally, control experiments in which ATRP using unbound initiators was carried out in the presence of unfunctionalized SWNTs, under identical conditions to our SWNT-initiated polymerizations, resulted in the production of free polymers having broad polydispersities (PDI > 2.5) and higher than expected molecular weights. This indicates that the presence of the nanotubes prevents the polymerization from being a "living" process. Addition of $CuBr_2$ rather than sacrificial initiator to these experiments similarly did not achieve any improved livingness, again resulting in polymers having broad polydispersities (PDI ~ 3.45). These results indicate that the presence of carbon nanotubes causes a decrease in the concentration of the persistent radicals in solution,[105] thereby decreasing the degree of control over the polymerization process. Recently, it has been shown that radical species, produced when benzoyl peroxide is decomposed in the presence of alkyl iodides, can be used to functionalize the sidewalls of carbon nanotubes.[106] In these reactions, the nanotubes act as radical scavengers, thereby removing radical species from solution. We believe that similar reactions may be occurring in our experiments, resulting in the elimination of the radical capping agents that are necessary for control of the polymerization process.

However, recently Yan[107] and Herrera[108] groups reported that they functionalized MWNTs and SWNTs by ATRP, respectively, using a "grafting from" method which is similar to our approach and obtained a controlled polymerization results. The conclusion of Yan's work was based on the observation that the thickness of the polymer layer in the functionalized MWNT can be well-controlled by the feed ratio of MMA to MWNT-Br and the ATRP of hydroxyethyl methacrylate (HEMA) using MWNT-PMMA as the macroinitiator was successfully performed. The ATRP results using nanotube based macroinitiators are determined by various factors including reaction temperature, ATRP ligand, solvent, initiator loading, etc. In their system, they attached ATRP initiators to the ends and defects of MWNTs, the reaction temperature was 60°C and the ligand they used was N,N,N',N",N"-pentamethyldiethylenetriamine (PMDETA). It would be worthwhile to see if the ATRP using our macroinitiator, under the same conditions as theirs, is controlled or not. It should be noted that in their research they did not cleave the polymer from MWNTs and did not get the molecular weight and polydispersities of the attached polymers. In Herrera's work, they polymerized n-butyl methacrylate (nBMA) from the ends and defect sites of SWNTs in the presence of small quantities of free initiators and found that the molecular weight of free poly(n-butyl methacrylate) (PnBMA) increased linearly with nBMA monomer conversion. Although researchers often assume that the molecular weights of free polymers are the same as those of the attached polymers, it is better to get the exact molecular weights of the attached polymers to see whether the polymerization initiated on the SWNTs is actually controlled or not.

3.4.3 Solubility of Polymerized SWNTs.

Considering our initial goal of improving nanotube solubility and processibility, we investigated the solubility of the polymerized SWNTs in various organic solvents. We were disappointed to find that the PMMA chains attached in our initial experiments did not impart any enhanced solubility (Figure 3-13) to the nanocomposites in CH_2Cl_2, $CHCl_3$, THF, acetone, or even DMF and DMSO. Considering the high solubility of PMMA in organic solvents such as THF, it is surprising that no solubility enhancement was observed for these samples. One possible explanation for the poor solubility of the nanocomposites is the potential for crosslinking to occur during polymerization as a result of radical coupling of the growing polymer chain ends. Such crosslinking can occur between chain ends of polymers growing from a single nanotube, or between polymers growing from different SWNTs, possibly comprising a single nanotube bundle. The former case would prevent polymers from extending into solution, decreasing their solubility. In the latter case, large networks of nanotubes interconnected by polymer chains could be formed, and would be too large to allow for effective solubilization. Although these structures were not soluble, TEM comparison of the polymerized nanotubes to control experiments in which the initiators were not bound to the nanotubes clearly demonstrated a significant difference in nanotube dispersion (Figure 3-14). In the control experiments, the nanotube distribution was not nearly as homogeneous as it was in the samples where polymers were covalently attached to the nanotubes. The control experiments exhibited many regions containing only clusters of carbon nanotubes with no associated polymer, whereas the covalently functionalized nanotubes were very evenly distributed throughout the sample. This is consistent with the previously observed phase separation of nanotubes from bulk polymers in simple mixtures of the two materials.[109] This phase separation is caused by the substantial van der Waals interactions that occur between nanotubes, and precludes the homogeneous dispersion of unfunctionalized nanotubes in bulk polymers.

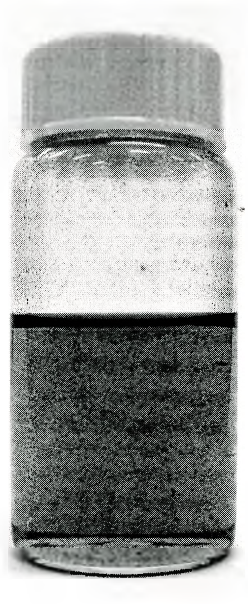

Figure 3-13. suspension of PMMA-SWNT samples in THF.

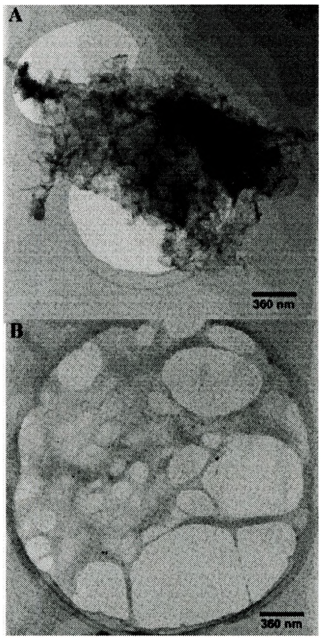

Figure 3-14. TEM (A) a sample of the mixture of free PMMA with SWNTs and (B) a sample of polymerized SWNTs.

3.5 Experimental

General. Single-walled carbon nanotubes (SWNTs) were purchased from Carbon Nanotechnologies, Inc. (Houston, TX). N-(4-hydroxyphenyl) glycine was purified by recrystalization in distilled H_2O. Methyl methacrylate (MMA) was purified by passing through basic alumina column and stored in the fridge. All other reagents and solvents were purchased from commercial suppliers and used as received. FTIR was performed on a Bio-Rad FTS-40 instrument. All samples were prepared as pellets using spectroscopic grade KBr in a Carver press at 15 000 psi. Laser Raman spectroscopy was performed on a Jobin-Yvon SR-3000 macro/micro-Raman spectrometer operating with a 514.5 nm Ar ion laser (Spectra Physics). Atomic Force Microscopy was done using a Digital Instruments NanoScope IIIa Multimode AFM, with samples prepared by drop casting sample solutions or suspensions on either HOPG or freshly cleaved mica substrates. The images were recorded with standard tips in tapping mode at a scan rate of 0.5 Hz. TEM analysis was performed using a Philips CM12 operating at 120 keV. NMR was performed on a Bruker 200 MHz instrument in $CDCl_3$. Differential scanning calorimetry (DSC) was performed on a TA 2100 Modulated Differential Scanning Calorimeter with a temperature gradient of 15 degrees/min. Ultrasonication was done in a Banson Ultrasonics B1510 bath sonicator. Filtration was done through either a 100 nm-pore polycarbonate membrane (Millipore), a 200 nm-pore teflon membrane (Millipore). Molecular weights and polydispersity index (PDI) were estimated by gel permeation chromatography (GPC) using a

Waters 2695 Separations Module equipped with a Waters 2996 Photodiode Array Detector, a Waters 2414 Refractive Index Detector and a Waters 2475 Multi λ Fluorescence Detector. Polystyrene standards were used for calibration. Tetrahydrofuran (THF) was used as the eluent at a rate of 1.0 mL/min. The concentrations of the soluble polymer functionalised SWNTs were calculated from the UV/Vis absorption results obtained from the Cary 50 Bio UV-Visible Spectrophotometer.

Shortening and purification of SWNTs. A 250 mL flask charged with 50 mg of SWNTs and 100 mL of a H_2SO_4/HNO_3 (v:v 3/1) solution was sonicated for 2 hours. Then the mixture was diluted in a 500 mL beaker with 200 mL of distilled water. After cooling down, the diluted solution was filtered through 100 nm-pore Polycarbonate membrane. The black material collected from the membrane was further treated by stirring with 50 mL H_2SO_4/H_2O_2 (9/1) in a 250 mL flask for 30 min at room temperature. Another 50 mL H_2SO_4/H_2O_2 (9/1) was added and the solution was sonicated for 5 min. After dilution using 200 mL of distilled water in a 500 mL beaker, the solution was filtered through a 100 nm-pore Polycarbonate membrane. The resulting mat of SWNTs was washed thoroughly using 10 mM NaOH solution and distilled water until the pH of the filtrate was 7. The purified SWNTs were then dried under vacuum overnight. IR (KBr pellet): 1741(s), 1627 (m) cm^{-1}.

Synthesis of Macroinitiator (2). *Step 1*: 30 mg of purified SWNTs, 50 mg (3.0×10^{-4} mol) of N-(4-hydroxyphenyl) glycine and 2 mL (0.012 mol) of octyl aldehyde were dispersed in 50 mL of DMF in a 250 ml flask. The mixture was stirred at 130°C under argon for 5 days with further addition of 50 mg (3.0×10^{-4} mol) of N-(4-hydroxyphenyl) glycine once every 24 h. At the end of this process, the product was collected by filtering through a 200 nm-pore Teflon membrane, and was then washed thoroughly with CH_2Cl_2 (100 mL), THF (50 mL), and methanol (50 mL), and finally dried under vacuum overnight. IR (KBr pellet): 3437 (s), 2926-2855 (m), 1634 (s) cm^{-1}.

Step 2: The macroinitiators were produced by the coupling reaction of 2-bromoisobutyryl bromide with the phenol group functionalized SWNTs (from step 1). Into a 50 mL flask were added, 20 mL of anhydrous DMF, 20 mg of SWNTs, 1 mL (8 mmol) of 2-bromoisobutyryl bromide and 1 mL (7 mmol) triethylamine (1 mL). The mixture was stirred at 70°C under argon for 48 h. The product was isolated by filtration through a 200 nm-pore Teflon membrane and thoroughly washed with CH_2Cl_2 (100 mL), THF (50 mL), and methanol (50 mL), then dried under vacuum overnight. IR (KBr pellet): 2918-2849 (m), 1759 (s), 1652-1609 (m) cm^{-1}.

Synthesis of poly(methyl methacrylate)-functionalized nanotubes (3). 4 mg of SWNT macroinitiator (**2**) was dispersed in 8 mL of DMF, 3 mL of deionized H_2O and 3 mL (28 mmol) MMA in a 25 mL flask. The mixture bubbled with N_2 for 30 min was transferred using a cannula to another 25 mL flask charged with 175 mg 2, 2'-dipyridyl (1.12 mmol) and 40mg CuBr (0.28 mmol) full of argon. The polymerization was carried out at room temperature for 24 h. The polymer functionalized SWNTs were purified by washing with THF, CH_2Cl_2 and methanol successively during filtration through a 200 nm-pore teflon membrane. The isolated grey product from the membrane was dried under vacuum overnight. IR (KBr pellet): 2999-2954 (m), 1733 cm^{-1} (s).

Cleavage of poly(methyl methacrylate) from the SWNTs. In a typical cleavage experiment, 30 mg of PMMA functionalized SWNTs were mixed with 7 mL of distilled CH_2Cl_2 in a 25 mL flask, followed by the addition of 2 mL of a saturated solution of $NaHCO_3$ in methanol, and a further 100 mg of $NaHCO_3$. The mixture was stirred overnight at room temperature. The cleaved polymer was isolated by filtering through a 200 nm-pore teflon membrane while washing with THF thoroughly to get rid of the SWNTs and $NaHCO_3$. After condensation the filtrate solution in vacuo, the cleaved polymer was precipitated into 20 mL of MeOH in a 100 mL beaker and isolated by filtration on a medium porosity glass frit. The product was dried under vacuum overnight. ^1H NMR (200 MHz, $CDCl_3$): δ 3.59, δ 1.81-1.87, δ 0.84-1.02 ppm.

Chapter 4 Polymerization of t-butyl acrylate from SWNTs

4.1 Overview

In order to further explore the possibility of solubilizing SWNTs, we chose to investigate the polymerization of t-butyl acrylate (t-BuA). We postulated that the bulkier t-butyl group on each monomer unit might enhance the solubility of the polymerized tubes, even if crosslinking due to radical coupling of chain ends still occurred. In addition, it is well known that removal of the t-butyl groups can be efficiently performed under acidic conditions, leading to the formation of poly (acrylic acid), which is a water-soluble polymer. The prospect of modulating the solubility of the nanocomposites through post-polymerization chemistry was appealing and was a motivating factor for switching to this particular monomer.

4.2 Polymerization of t-BuA using the macroinitiators

The SWNT macroinitiator **2** was used to polymerize t-BuA under identical conditions to the polymerization of MMA (Scheme 4-1). After polymerization, the SWNT nanocomposites were isolated using identical procedures as for the PMMA-functionalized nanotubes.

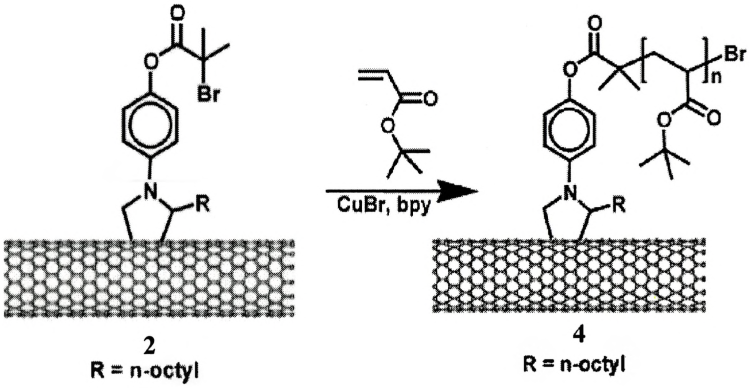

Scheme 4-1. Polymerization of t-BuA using the ATRP macroinitiators.

DSC performed on this sample indicated a *T*g of 46.6 °C, which is slightly higher than the *T*g of poly(*tert*-butyl acrylate), observed at 43.1 °C. The result is as expected because the mobility of polymer chains was constrained by the SWNTs.

The IR and Raman spectra for this sample are given in Figure 4-1 and Figure 4-2, respectively. Characteristic IR stretches at ca. 1730 cm^{-1} and ca. 2950 cm^{-1} indicate the presence of polymer, while Raman signals at ca. 200 cm^{-1} and ca. 1590 cm^{-1} correspond to the radial breathing modes and the tangential modes of the SWNT. In addition, a significant disorder peak at 1338 cm^{-1} is apparent, corresponding to the presence of sp^3-hybridized carbon atoms within the nanotubes formed as a result of the functionalization process. This disorder peak is proportional to the extent of nanotube functionalization.

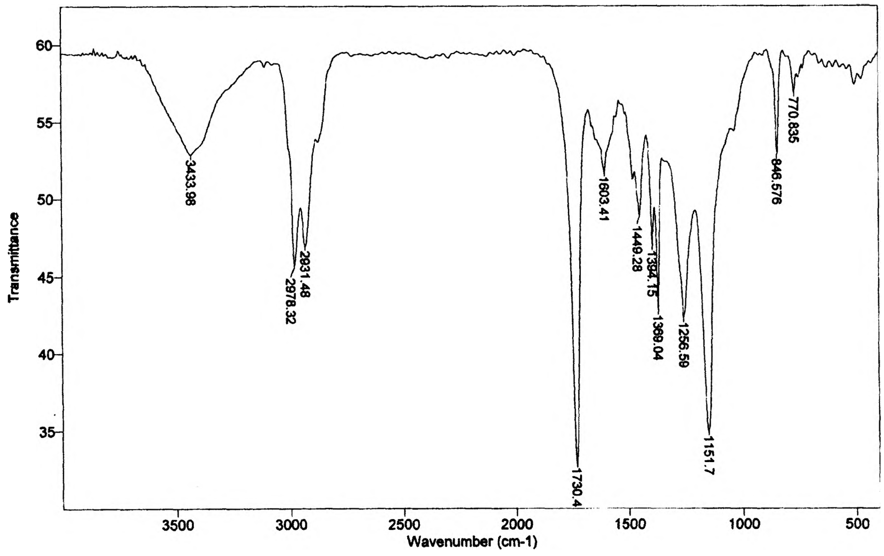

Figure 4-1. FT-IR analysis of poly(t-butyl acrylate) functionalized SWNTs.

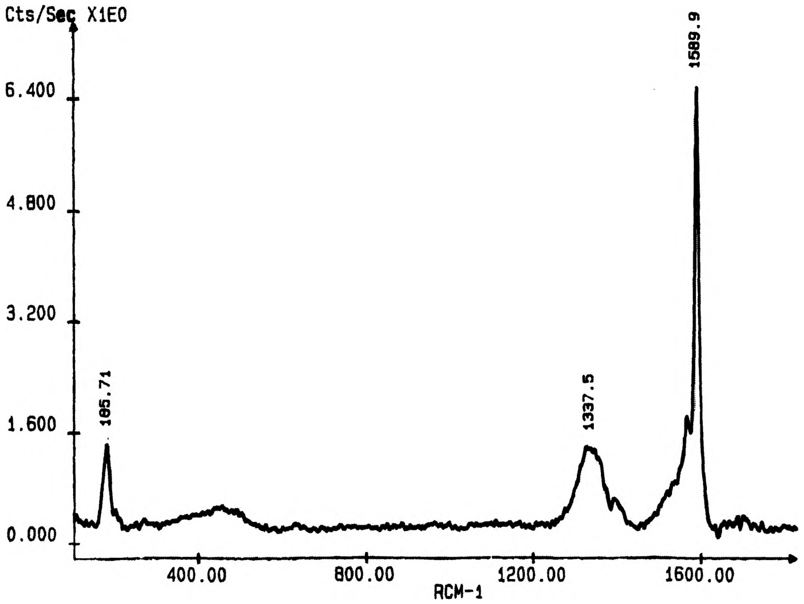

Figure 4-2. Raman spectrum of poly(t-butyl acrylate) functionalized SWNTs .

Solution ^{1}H NMR (200MHz, $CDCl_3$) spectroscopy also provided evidence that the polymer is present within this material (Figure 4-3). Aliphatic proton signals were observed in the region between 0.8 and 1.8 ppm, corresponding to the polymer backbone protons as well as the t-butyl side chains. No signals corresponding to the aromatic protons of the phenol linker between the pyrrolidine ring and the polymer were observed due to the extremely low concentration and mobility of these groups within the structures.

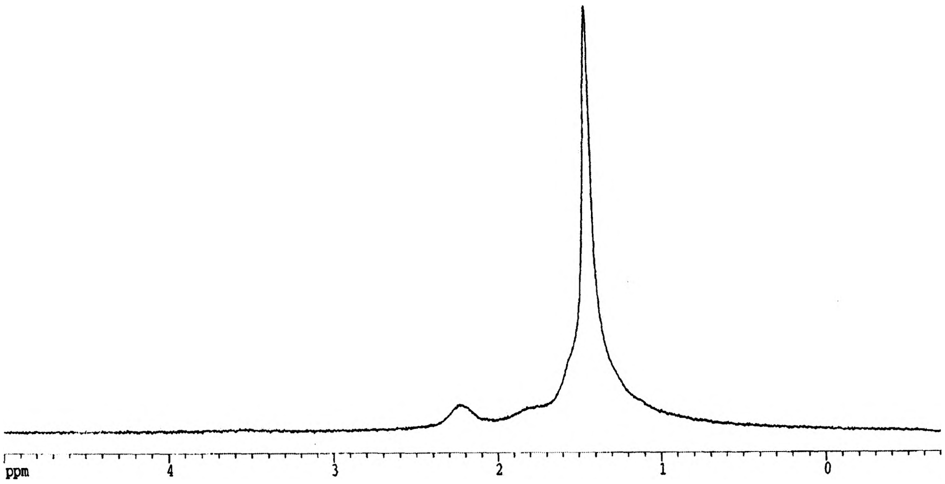

Figure 4-3. NMR spectrum of the PtBA-SWNTs sample.

4.3 Solubility of the PtBA-SWNTs samples

The poly(t-butyl acrylate) functionalized nanotubes (**4**) were found to be soluble in a range of organic solvents, including CH_2Cl_2, $CHCl_3$, and THF (Figure 4-4 A and B). Using UV/Vis absorption spectroscopy (Figure 4-5) at 500 nm and the reported specific extinction coefficient of $\varepsilon_{500} = 28.6\ cm^2/mg$,[98] the estimated nanotube concentration in the THF solution was 50.3 mg/L.

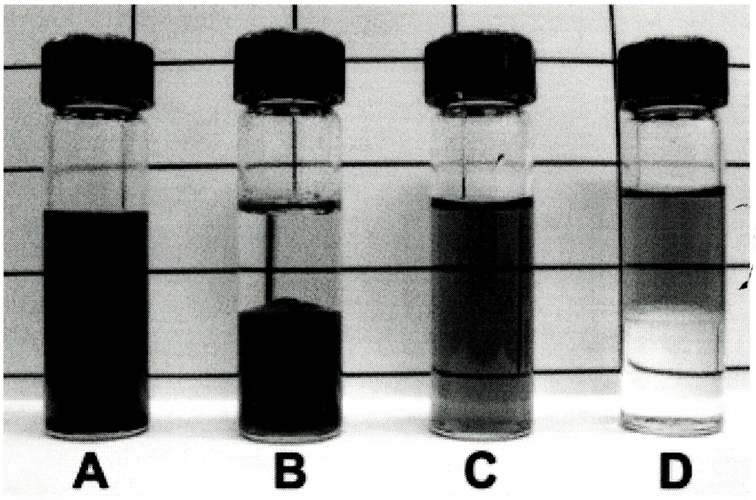

Figure 4-4. Solutions of polymerized nanotubes. (A) PtBA-SWNT sample in THF; (B) PtBA-SWNT sample in a mixture of H_2O/CH_2Cl_2; (C) PAA-SWNT sample in H_2O; (D) PAA-SWNT sample in a mixture of H_2O/CH_2Cl_2.

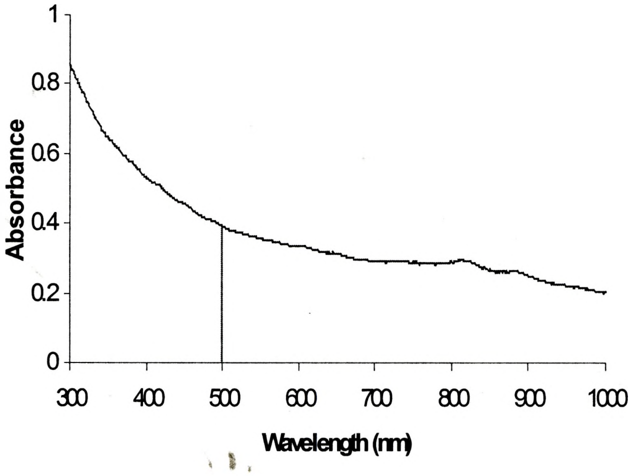

Figure 4-5. UV-vis absorptions PtBA-SWNTs sample in THF solution.

4.4 Conversion of poly(t-butyl acrylate) to poly(acrylic acid)

The solubility of the poly(t-butyl acrylate) functionalized nanotubes could be drastically affected by removal of the t-butyl groups. This was accomplished by stirring the nanotubes in 10% trifluoroacetic acid (TFA)/CH_2Cl_2 solutions (v/v) for 12 h (Scheme 4-2). Upon evaporation of the solvent and acid, the resulting PAA-functionalized nanotubes (**5**) were found to be soluble in a 10 mM NaOH solution (Figure 4-4 C and D), and completely insoluble in organics such as CH_2Cl_2. UV/Vis measurements (Figure 4-6) were again used to estimate the nanotube concentration, which was found to be approximately 19.7 mg/L in this solution. Furthermore, the solution remained stable for several weeks, with no apparent precipitation of the polymerized SWNTs.

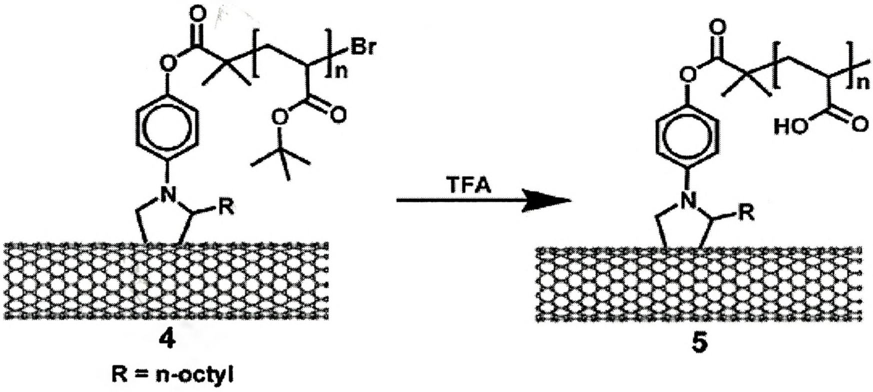

Scheme 4-2. Conversion of poly(t-butyl acrylate) to poly(acrylic acid).

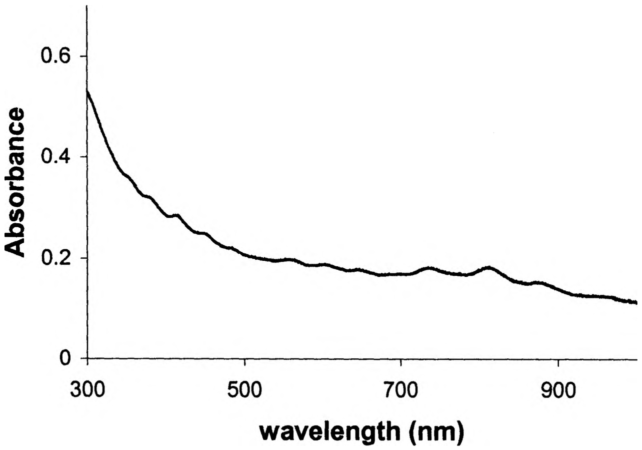

Figure 4-6. UV-vis absorptions PAA-SWNTs sample in H_2O solution.

The IR spectrum for this sample is given in Figure 4-7. Characteristic IR stretches at ca. 1717 cm^{-1} and ca. 2950 cm^{-1} indicate the presence of polyacrylic acid.

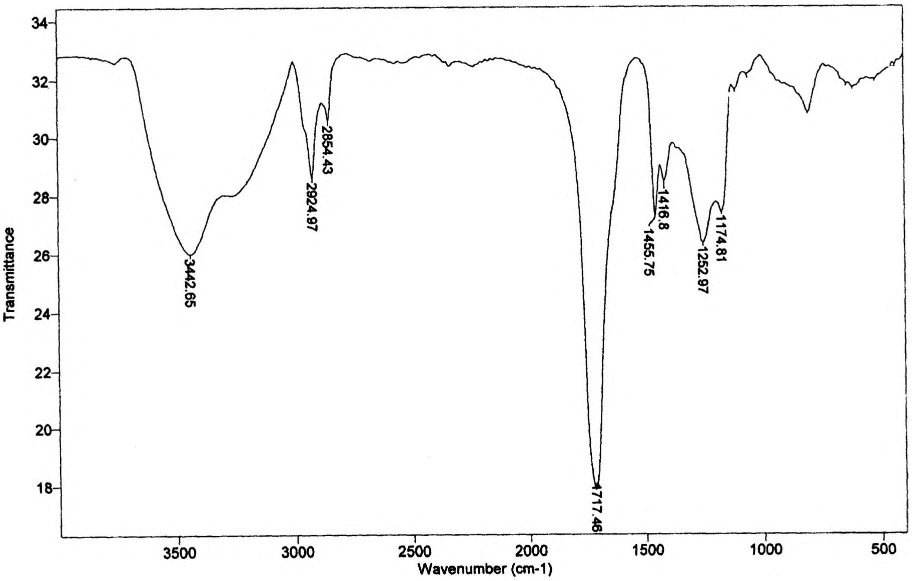

Figure 4-7. FT- IR spectrum of PAA-SWNTs sample.

In summary, in this chapter we discussed the results of polymerization of t-BuA using the ATRP macroinitiators and the conversion of poly(t-butyl acrylate) to poly(acrylic acid). It was shown that the solubility of SWNTs can be altered by changing the types of polymers attached to the SWNTs.

4.5 Experimental

General. Single-walled carbon nanotubes (SWNTs) were purchased from Carbon Nanotechnologies, Inc. (Houston, TX). N-(4-hydroxyphenyl) glycine was purified by recrystalization in distilled H_2O. t-Butyl acrylate was purified by passing through basic alumina column and stored in the fridge. All other reagents and solvents were purchased from commercial suppliers and used as received. FTIR was performed on a Bio-Rad FTS-40 instrument. All samples were prepared as pellets using spectroscopic grade KBr in a Carver press at 15 000 psi. Laser Raman spectroscopy was performed on a Jobin-Yvon SR-3000 macro/micro-Raman spectrometer operating with a 514.5 nm Ar ion laser (Spectra Physics). Differential scanning calorimetry (DSC) was performed on a TA 2100 Modulated Differential Scanning Calorimeter with a temperature gradient of 15 degrees/min. Ultrasonication was done in a Banson Ultrasonics B1510 bath sonicator. Filtration was done through either a 100 nm-pore polycarbonate membrane (Millipore), a 200 nm-pore teflon membrane (Millipore). The concentrations of the soluble polymer functionalised SWNTs were calculated from the UV/Vis absorption results obtained from the Cary 50 Bio UV-Visible Spectrophotometer.

Shortening and Purification of SWNTs. A 250 mL flask charged with 50 mg of SWNTs and 100 mL of a H_2SO_4/HNO_3 (v/v: 3/1) solution was sonicated for 2 hours. The mixture was then diluted with 200 mL of distilled water. After cooling to room temperature, the diluted solution was filtered through a 100 nm-pore polycarbonate membrane. The black material collected from the membrane was further treated by stirring with 50 mL H_2SO_4/H_2O_2 (9/1) in a 250 mL flask for 30 min at room temperature. Another 50 mL of H_2SO_4/H_2O_2 (9/1) was added and the solution was sonicated for 5 min. After dilution using 200 mL of distilled water, the solution was filtered through a 100 nm-pore polycarbonate membrane. The resulting mat of SWNTs was washed thoroughly using first a 10 mM NaOH solution, and then distilled water until the pH of the filtrate was 7.

Synthesis of poly(*tert*-butyl acrylate)-functionalized nanotubes (4). Under the same conditions as the polymerization of MMA, *tert*-butyl acrylate (3 mL) was polymerized in the presence of **2**. Centrifugation (5000 rpm, 10 min) was used instead of filtration due to the tackiness of the product. Suspensions of the product in THF were centrifuged 3 times, decanting the solvent after each centrifugation cycle to remove any free polymer that may have formed in the reaction. The black film was dried under vacuum overnight. ^1H NMR (200MHz, $CDCl_3$): δ 2.23 (broad), 1.70 (broad), and 1.43 (broad) ppm. IR (KBr pellet): 2978-2931 (m), 1730 cm^{-1} (s).

Synthesis of poly(acrylic acid)-functionalized SWNTs (5). Poly (*tert*-butyl acrylate) (P*t*BA)-functionalized SWNTs (10 mg) were deprotected by stirring in a mixture of trifluoroacetic acid (TFA) (1 mL) and anhydrous CH_2Cl_2 (10 mL) at room temperature under argon for 12 h. The product was isolated by flowing nitrogen gently into the flask to remove the TFA and CH_2Cl_2. IR (KBr pellet): 2924-2854 (m), 1717 cm^{-1} (s).

Chapter 5 Functionalization of SWNTs with polystyrene

5.1 Overview

Besides the "grafting from" method discussed in the previous chapters, polymers are often attached onto the SWNTs through a 'grafting to' approach in which the carboxylic acid groups at the nanotube ends and defect sites are utilized to anchor the polymer chains onto the SWNTs. These polymers are required to have functional groups, such as $-NH_2$ and -OH, to form ester or amide bonds with the carboxylic groups.[52] In these methods, the grafting density of the attached polymers is low because the amount of carboxylic groups at the ends and defect sites of SWNTs is limited.

It has recently been shown that the radical coupling chemistry that has been widely applied to the functionalization of C_{60}[110] is also applicable to carbon nanotubes[111]. The reaction site of this approach is on the sidewall of SWNTs, therefore it is possible to obtain high polymer loaded functionalized SWNTs composites.

In this chapter, we report the sidewall functionalization of SWNTs through polystyryl radicals thermally produced from polystyrene (PS) which was made by stable free radical polymerization (SFRP). There are 2 reasons we chose SFRP to make polystyrene. First, it is easy to make polystyrene with controlled molecular weights and lower polydispersity by using SFRP; second, at 125°C polystyrene terminated with nitroxide homolytically dissociates into stable nitroxide free radical and carbon centered radicals, which can be trapped by SWNTs to form polymer functionalized SWNT composites. The functionalized composite was fully characterized using techniques such as IR, Raman, NMR, UV-vis, TEM, AFM.

5.2 Synthesis and characterization of polystyrene

In the polymerization of styrene by SFRP (Scheme 5-1), compound **1** (2,2,5,5-tetramethyl-3-(1-phenylethoxy)-4-chloromethyl-phenyl-3-azahexane) was chosen as the initiator (Scheme 5-1). It was synthesized following the procedure reported by Hawker and co-workers.[79] Acetic anhydride was used as an additive for SFRP to obtain a relatively fast polymerization rate and narrow polydispersity.[87] The polymerizations were performed in bulk at 125°C. The resulting polymer products were isolated and purified by precipitation into methanol, filtered and dried under vacuum overnight.

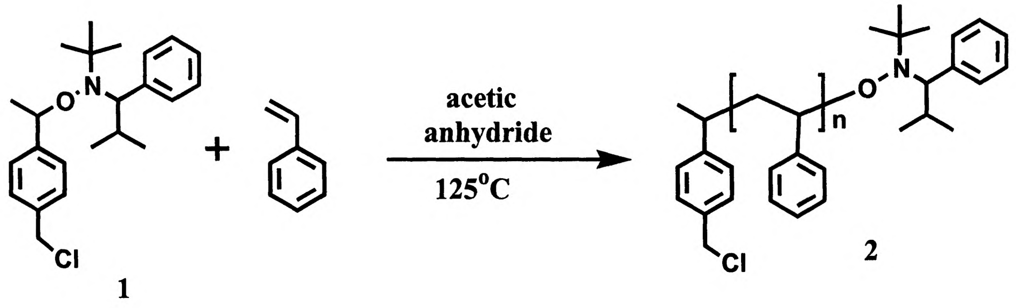

Scheme 5-1. Polymerization of styrene by SFRP.

By varying the styrene to initiator ratio, PS with desired molecular weight and narrow polydispersity was prepared. The product was analyzed by gel permeation chromatography, measured against commercial PS standards. Figure 5-1 shows GPC results for polystyrene samples. We can see that all samples give sharp peaks in GPC results, except that there is a small shoulder for sample 4, which might be due to the coupling termination. The molecular weights and PDI results of different polystyrene samples are shown in Table 5-1. PDI values of the all the samples are less than 1.2, which means that the polymerization is well controlled. It should be noted that the conversion in experiment 4 was about 60%.

Table 5-1. Mn, PDI and styrene:initiator ratio for different polymerizations.

Experiment No.	Mn (g/mol)	Mn (theo.) (g/mol)	PDI	Styrene: initiator ratio
1	1894	2080	1.08	20:1
2	3354	4160	1.17	40:1
3	6428	10400	1.09	100:1
4	11149	10400	1.10	100:1

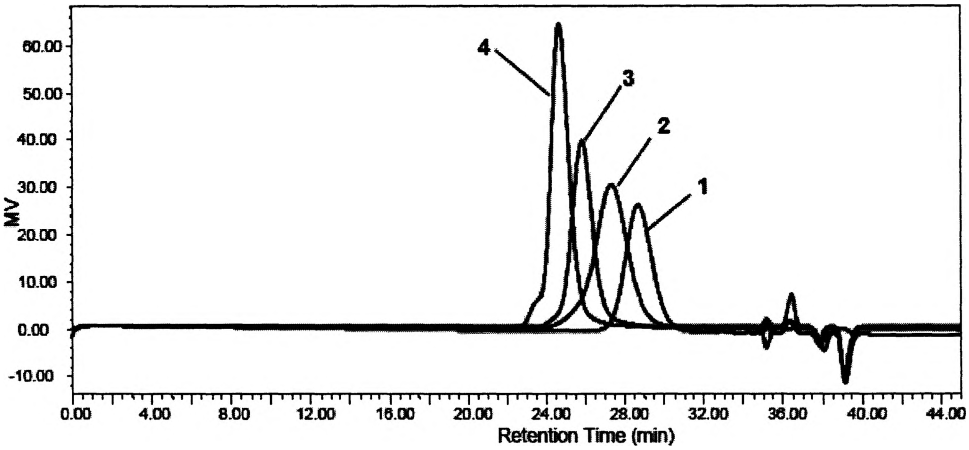

Figure 5-1. GPC results of PS prepared by SFRP. Mn=1894, PDI=1.08 (1); Mn=3354, PDI=1.17 (2); Mn=6428, PDI=1.09 (3); Mn=11149, PDI=1.10 (4).

5.3 Functionalization of SWNTs with polystyrene

In a typical reaction, addition of the nitroxide-terminated polystyrene **3** (500 mg) and acetic anhydride (50 µL) to a suspension of shortened SWNTs (10 mg) in DMF (10 mL), followed by bubbling with N_2 for 30 min and stirring at 125°C under argon for three days, resulted in the functionalized SWNT-PS composite (Scheme 5-2). After the reaction mixture was cooled down to room temperature, it was filtered through a Teflon membrane with a pore size of 200 nm and washed with a large amount of CH_2Cl_2 (300 mL), $CHCl_3$ (200 mL), and THF (200 mL) until there was no free PS left, which was determined by thin layer chromatography (TLC).

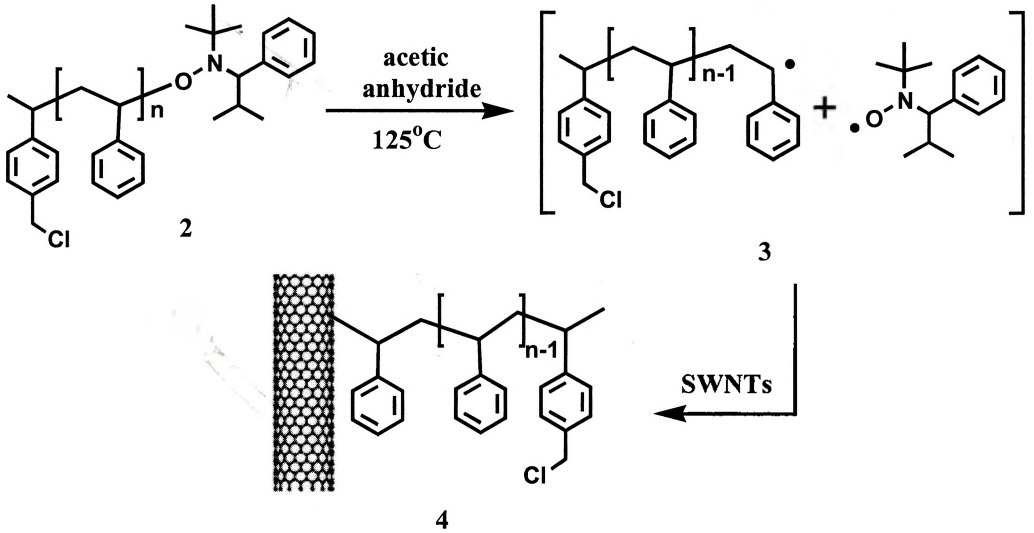

Scheme 5-2. Functionalization of SWNTs with PS by radical coupling.

It was found that the functionalization reaction drastically affected the solubility characteristics of the resulting PS-functionalized SWNTs. The shortened SWNTs exhibit some solubility in water prior to polymer functionalization. However, after functionalization with PS, the composite **4** became insoluble in H_2O but highly soluble in a range of organic solvents (Figure 5-2), including CH_2Cl_2, THF, $CHCl_3$. The high solubility allowed further purification of the composites by simple column chromatography, through which we could observe a dark layer of silica containing our immobilized nanotube conjugates while all free polymer was removed when using CH_2Cl_2 as the eluent. A control experiment, in which the SWNTs were reacted with the alkoxyamine initiator alone, under identical conditions and concentrations to the polymer reactions described above, resulted in no increase in the solubility of the resulting SWNTs.

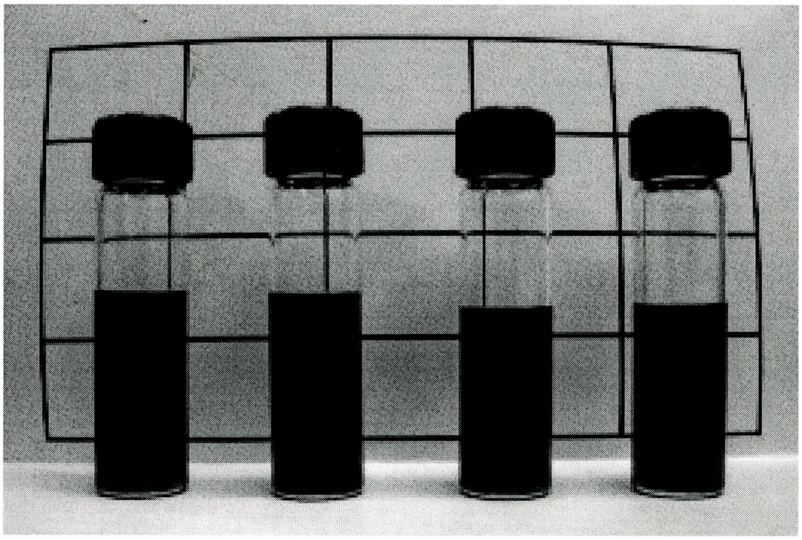

Figure 5-2. THF solutions of the PS-SWNTs functionalized with different PS molecular weights. Mn = 1,894; 3,375; 6,428; 11,149 g/mol (from left to right).

Following the same method as chapter 3, the degree of SWNT solubility in various solvents as a result of functionalization was also estimated by UV/Vis spectroscopy using 0.028 as the extinction coefficient. The highest solubility was found to be in THF, with nanotube concentrations in excess of 200 mg/L for all the synthesized samples. Figure 5-3 shows the UV/Vis absorbance of PS-SWNTs in THF.

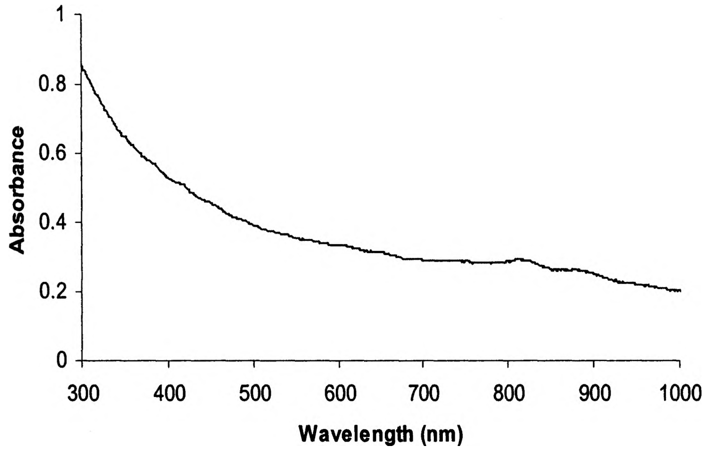

Figure 5-3. UV/Vis spectrum of PS (Mn = 3,354 g/mol) functionalized SWNTs in THF (saturated solutions were diluted 10-fold prior to measurement).

Due to this relatively high solubility, solution-phase ^{1}H NMR spectroscopy could be utilized to study the polymer portion of the sample. Figure 5-4A depicts the ^{1}H NMR spectra of the PS sample (Mn = 3,354 g/mol) used in nanotube functionalization and the PS-functionalized SWNTs. The two spectra are similar, clearly illustrating that PS was, indeed, attached to the surface of carbon nanotubes. Both of the spectra show the expected aromatic signals for PS, at δ = 7.07 and 6.56 ppm (broad), as well as the backbone signals at δ = 1.84 and 1.42 ppm. The relatively small peaks below 1.0 ppm in Figure 5-4A are due to the alkoxyamine initiator fragments at the ends of the polymer chains. These signals remain after functionalization (Figure 5-4B), indicating that some nitroxide radical fragments may have also coupled to the SWNTs during the course of the reaction.

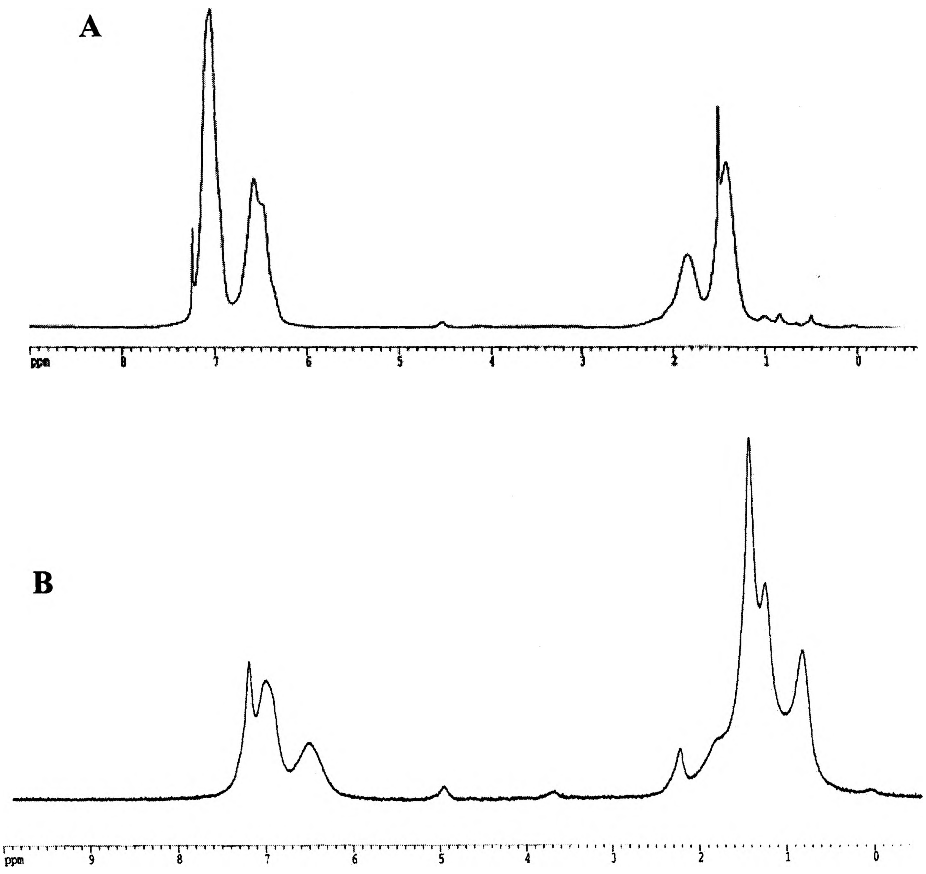

Figure 5-4. ^{1}H NMR spectra of (A) PS and (B) PS functionalized SWNTs.

This same material was analyzed by Raman spectroscopy and exhibited the characteristic signals at ca. 267 cm^{-1} and ca. 1590 cm^{-1} corresponding to the radial breathing modes and the tangential G mode of the SWNTs (Figure 5-5). In addition, a very small disorder peak at ca. 1276 cm^{-1} corresponding to the presence of sp^3-hybridized carbon atoms within the nanotubes could be observed. The Raman results indicate that, although the nanotube solubility has increased dramatically as a result of the functionalization, the overall nanotube chemical structure has not been significantly altered.

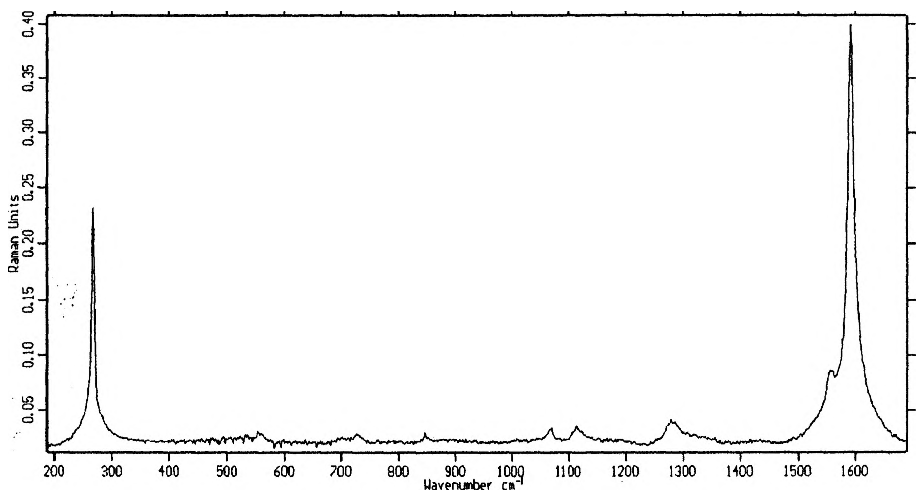

Figure 5-5. Raman spectrum of PS functionalized SWNTs.

Analysis of the polystyrene (Mn = 3,354 g/mol) functionalized SWNTs by AFM revealed that the topological morphology of these materials is significantly altered when compared to unfunctionalized SWNTs. Figure 5-6A depicts a sample of shortened SWNTs prior to functionalization, prepared by spin casting from a DMF suspension onto freshly cleaved mica, where small nanotube bundles having heights in the range of 1-5 nm can be observed. After polymer functionalization, the nanotube sample was spin cast from a THF solution, again onto freshly cleaved mica, and revealed nanotube bundles that were coated or closely associated with an amorphous material, presumably polystyrene (Figure 5-6B). In this sample, individual features reached heights of up to 15 nm. Interestingly, changing the casting solvent to $CHCl_3$ resulted in a completely different surface topology, where the nanotube bundles seemed to be embedded in a polymeric matrix (Figure 5-6C). It is presumed that differences in the nanotube polymer vs. nanotube-solvent interactions are responsible for the observed topological differences (SWNTs have been shown to be more soluble in $CHCl_3$ than in THF). TEM analysis of the polymer-functionalized structures also revealed the presence of nanotube bundles coated with amorphous polymeric material (Figure 5-6D). In some areas, it is possible to observe bare nanotube bundles spanning the gap between two polymer-coated regions.

In conclusion, in this chapter we reported the results of functionalization of SWNTs with polystyrenes with well defined molecular weights using the radical coupling reaction. The solubility of SWNTs in organic solvents was increased dramatically and the composites were characterized by AFM, TEM, Raman, UV-vis and NMR.

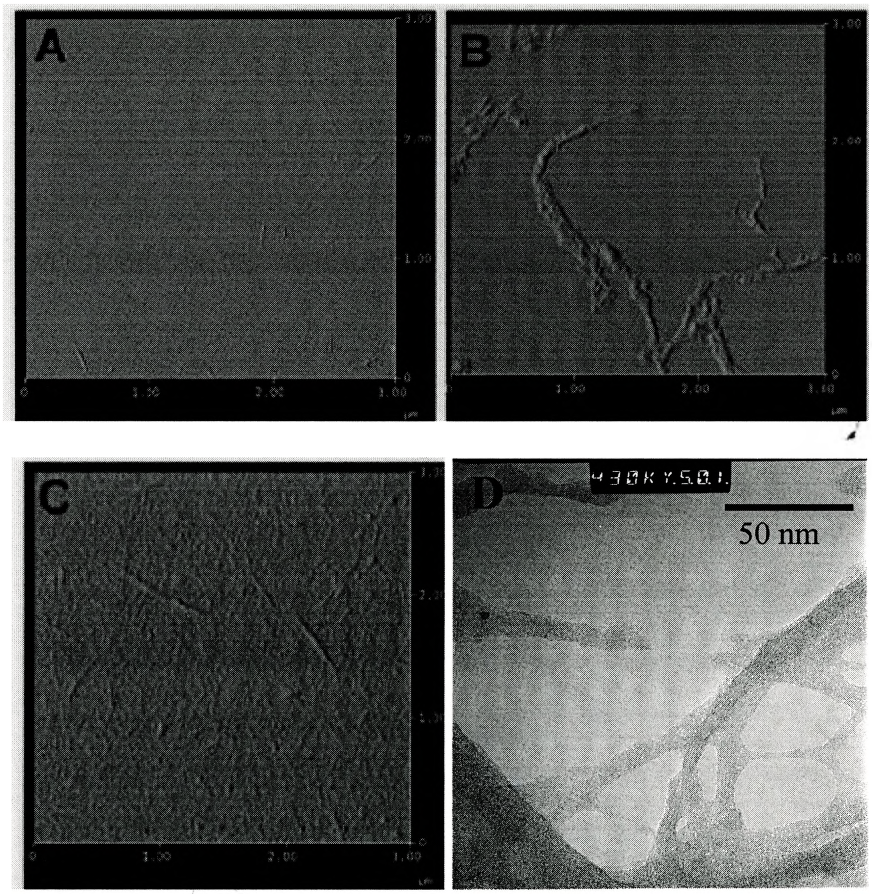

Figure 5-6. AFM image of purified SWNTs (A); AFM image of PS functionalized SWNTs spin-cast from THF solution (B); AFM image of PS functionalized SWNTs spin-cast from $CHCl_3$ solution (C); TEM image of PS functionlized SWNTs (D).

5.4 Experimental

General. Single-walled carbon nanotubes (SWNTs) were purchased from Carbon Nanotechnologies, Inc. (Houston, TX). Styrene was purified by passing through basic alumina and stored in the fridge. All other reagents and solvents were purchased from commercial suppliers and used as received. Raman spectra were obtained using a Renishaw InVia Raman Microscope equipped with an 1800 grooves/mm grating, CCD detector and He-Ne Laser (632.8 nm). Atomic Force Microscopy was done using a Digital Instruments NanoScope IIIa Multimode AFM, with samples prepared by spincoating sample solutions or suspensions on freshly cleaved mica substrates. The images were recorded with standard tips in tapping mode at a scan rate of 1.0 Hz. TEM analysis was performed using a Philips CM12 operating at 120 keV. NMR was performed on a Bruker 200 MHz instrument in $CDCl_3$. Filtration was done through either a 100 nm-pore polycarbonate membrane (Millipore) or a 200 nm-pore teflon membrane (Millipore). Polymer molecular weight and polydispersity index (PDI) were estimated by gel permeation chromatography (GPC) using a Waters 2695 Separations Module equipped with a Waters 2996 Photodiode Array Detector, a Waters 2414 Refractive Index Detector, a Waters 2475 Multi λ Fluorescence Detector, and four Polymer Labs PLgel individual pore size columns. Polystyrene standards were used for calibration, and tetrahydrofuran (THF) was used as the eluent at a flow rate of 1.0 mL/min. The concentrations of the soluble polymer functionalized SWNTs were calculated from UV-vis absorption spectra measured using a Cary 50 UV-vis Spectrophotometer.

Shortening and Purification of SWNTs. A 250 mL flask charged with 50 mg of SWNTs and 100 mL of a H_2SO_4/HNO_3 (v/v: 3/1) solution was sonicated for 2 hours. The mixture was then diluted with 200 mL of distilled water. After cooling to room temperature, the diluted solution was filtered through a 100 nm-pore polycarbonate membrane. The black material collected from the membrane was further treated by stirring with 50 mL H_2SO_4/H_2O_2 (9/1) in a 250 mL flask for 30 min at room temperature. Another 50 mL of H_2SO_4/H_2O_2 (9/1) was added and the solution was sonicated for 5 min. After dilution using 200 mL of distilled water, the solution was filtered through a 100 nm-pore polycarbonate membrane. The resulting mat of SWNTs was washed thoroughly using first a 10 mM NaOH solution, and then distilled water until the pH of the filtrate was 7.

Synthesis of polystyrene (2). In a typical reaction, a 25 mL round-bottom flask was charged with styrene (4.0 mL, 35.0 mmol), alkoxyamine initiator **1** (288 mg, 0.77 mmol), and acetic anhydride (0.03 mL, 0.32 mmol). The mixture was bubbled with N2 for 30 min and then the flask was placed into a 125°C oil bath. The reaction was allowed to proceed for 12 h and the product was dissolved in CH_2Cl_2 and then precipitated by dropwise addition of the solution into methanol. The precipitate was filtered and then dried under vacuum overnight. The product was analyzed by GPC, resulting in a Mn = 3354 g/mol and a PDI=1.17. By varying the ratio between styrene and the initiator, polystyrene with different molecular weights was obtained (Figure 5-1 and Table 5-1). ^{1}H NMR (200MHz, $CDCl_3$): δ 7.08 (broad), δ 6.59 (broad), δ 1.90 (broad) and δ 1.49 (broad) ppm.

Synthesis of polystyrene functionalized SWNTs (4). In a typical reaction, 10 mg of purified SWNTs, 0.05 mL (0.53 mmol) of acetic anhydride and 500 mg of polystyrene (Mn = 3354 g/mol) were dispersed in 15 mL of DMF in a 50 mL flask. The mixture was bubbled with N_2 for 30 min and then was stirred at 125°C under argon for 3 days. The product was collected by filtering through a 200 nm-pore Teflon membrane while washing thoroughly with CH_2Cl_2, THF, and methanol, and then dried under vacuum overnight. The mass of the isolated product increased by approximately 50%. ^1H NMR (200MHz, $CDCl_3$): δ 7.07 (broad), δ 6.56 (broad), and δ 1.25 - 1.43 ppm.

Chapter 6 Conclusions

Based on the research results we know that it is possible to functionalize shortened SWNTs with various polymers through "grafting from" or "grafting to" approaches.

6.1 "Grafting from" method

The 1,3-dipolar cycloaddition reaction on the surface of SWNTs using octanal and 4-hydroxyphenyl glycine resulted in phenol-functionalized tubes that could be further derivatized with 2-bromoisobutyryl bromide. The resulting modified SWNTs served as ATRP initiators for polymerization of MMA and *t*BuA, allowing for the formation of SWNT-polymer nanocomposites. IR, Raman, solid state ^{1}NMR and DSC analysis indicated that both nanotubes and polymers were present within the material isolated from the polymerization reaction. Unlike simple blends of polymers and nanotubes, the two components of our composites could not be separated from one another by extensive filtration and washing, indicating that they are covalently bound. Analysis of these structures by AFM and TEM provided further evidence for the formation of polymerized nanotubes and indicated that, in some instances, large nanotube bundles could be dissociated by the growth of polymers from their surface. Further, it was found that the attached polymers could be cleaved from the nanotubes. SEC analysis of the cleaved polymers demonstrated that the surface polymerizations were not controlled and resulted in extremely high molecular weight and PDI values. Attempts to add sacrificial initiators or $CuBr_2$ to the polymerizations were unsuccessful in improving control. Although the PMMA functionalized tubes were not soluble in organic solvents, the poly(*tert*-butyl acrylate)-functionalized tubes did exhibit good solubility in organic solvents such as CH_2Cl_2, $CHCl_3$, and THF. Upon removal of the *tert*-butyl groups, the resulting PAA functionalized tubes became soluble in aqueous solvents.

6.2 "Grafting to" method

An easier strategy was proposed to functionalize SWNT with polystyrene through the radical coupling reaction. Polystyrenes with desired molecular weights and lower polydispersity (less than 1.2) were prepared by SFRP and the resulted polystyrenes were utilized to functionalize the SWNTs under the similar condition to the SFRP of styrene. The functionalization of SWNTs with polystyrenes through the radical coupling reaction was successfully carried out. It was found that such polystyrene functionalized SWNTs acquire drastically improved solubility in various organic solvents, such as THF, DMF, CH_2Cl_2 and $CHCl_3$. The concentration of SWNTs in such organic solvents is up to 200 mg/L. It was confirmed that polystyrene was covalently bound to SWNTs based on the results of control experiments and the results from different characterization techniques such as AFM, TEM, Raman and NMR.

Reference

(1) Iijima, S. *Nature* **1991**, *354*, 56-58..

(2) Iijima, S.; Ichihashi, T. *Nature* **1993**, *363*, 603-605.

(3) Wei, B. Q.; Vajtai, R.; Choi, Y. Y.; Ajayan, P. M.; Zhu, H.; Xu, C.; Wu, D.; *Nano Lett.* **2002**; *2*; 1105-1107.

(4) Ajayan, P. M.; Ebbesen, T. W. *Rep. Prog. Phys.* **1997**, *60*, 1025-1062.

(5) Li, F.; Cheng, H. M.; Bai, S.; Su, G.; Dresselhaus, M. S. *Appl. Phys. Lett.* **2000**, *77*, 3161-3163.

(6) Yu, M. F.; Files, B. S.; Arepalli, S.; Ruoff, R. S. *Phys. Rev. Lett.* **2000**, *84*, 5552-5555.

(7) Wong, E. W.; Sheehan, P. E.; Lieber, C. M. *Science* **1997**, *277*, 1971-1975.

(8) Falvo, M. R.; Clary, G. J.; Taylor, R. M.; Chi, V.; Brooks, F. P.; Washburn, S.; Superfine, R. *Nature* **1997**, *389*, 582-584.

(9) Journet, C.; Maser, W. K.; Bernier, P.; Loiseau, A.; Chapelle, M. L.; Lefrant, S.; Deniard, P.; Lee, R.; Fischer, J. E. *Nature* **1997**, *388*, 756-758.

(10) Chopra, N. G. ; Luyken, H. ; Cherrey, K. ; Crespi, V.H. ; Cohen, M. L.; Louie, S.G.; Zettl, A. Sci*ence* **1995**, *269*, 966-968.

(11) Thess, A.; Lee, R.; Nikolaev, P.; Dai, H.; Petit, P.; Robert, J.; Xu, C.; Lee, Y. H.; Kim, S. G.; Rinzler, A. G.; Colbert, D. T.; Scuseria, G. E.; Tomanek, D.; Fischer, J. E.; Smalley, R. E. *Science* **1996**, *273*, 483-487.

(12) Fan, S.; Chapline, M. G.; Franklin, N. R.; Tombler, T. W.; Cassell, A. M.; Dai, H. *Science* **1999**, *283,* 512-514.

(13) Ren, Z. F.; Huang, Z. P.; Xu, J. W.; Wang, J. H.; Bush, P.; Siegal, M. P.; Provencio, P. N. *Science* **1998**, *282*, 1105-1107.

(14) Pan, Z. W.; Xie, S. S.; Chang, B. H.; Wang, C. Y.; Lu, L.; Liu, W.; Zhou, W. Y.; Li, W. Z.; Qian, L. X. *Nature* **1998**, *394*, 631-632.

(15) Nikolaev, P.; Bronikowski, M. J.; Bradley, R. K.; Rohmund, F.; Colbert, D. T.; Smith, K. A.; Smalley, R. E. *Chem. Phys. Lett.* **1999**, *313*, 91-97.

(16) Avouris, P. *Acc. Chem. Res.* **2002**, *35*, 1026-1034.

(17) Collins, P. G.; Avouris, P. *Sci. Am.* **2000**, *283*, 62-69.

(18) Dai, H. J. *Acc. Chem. Res.* **2002**, *35*, 1035-1044.

(19) Ajayan, P. M. *Chem. Rev.* **1999**, *99*, 1787-1799.

(20) Choi, W. B.; Chung, D. S.; Kang, J. H.; Kim, H. Y.; Jin, Y. W.; Han, I. T.; Lee, Y. H.; Jung, J. E.; Lee, N. S.; Park, G. S.; Kim, J. M. *Appl. Phys. Lett.* **1999**, *75*, 3129-3131.

(21) Dalton, A. B.; Collins, S.; Muñoz, E.; Razal, J. M.; Ebron, V. H.; Ferraris, J. P.; Coleman, J. N.; Kim, B. G.; Baughman, R. H. *Nature* **2003**, *423*, 703-704.

(22) Cadek, M.; Coleman, J. N.; Barron, V.; Hedicke, K.; Blau, W. J. *Appl. Phys. Lett.* **2002**, *81*, 5123-5128.

(23) Biercuk, M. J.; Llaguno, M. C.; Radosavljevic, M.; Hyun, J. K.; Johnson, A. T.; Fischer, J. E. *Appl. Phys. Lett.* **2002**, *80*, 2767-2769.

(24) Cadek, M.; Coleman, J. N.; Ryan, K. P.; Nicolosi, V.; Bister, G.; Fonseca, A.; Nagy, J. B.; Szostak, K.; Beguin, F.; Blau, W. J. *Nano Lett.* **2004**, *4*, 353-356.

(25) Tans, S. J.; Verschueren, A. R. M.; Dekker, C. *Nature* **1998**, *393*, 49-52.

(26) Deheer, W. A.; Chatelain, A.; Ugarte, D. *Science* **1995**, *270*, 1179-1180.

(27) Rinzler, A. G.; Hafner, J. H.; Nikolaev, P.; Lou, L.; Kim, S. G.; Tomanek, D.; Nordlander, P.; Colbert, D. T.; Smalley, R. E. *Science* **1995**, *269*, 1550-1553.

(28) Bachtold, A.; Hadley, P.; Nakanishi, T.; Dekker, C. *Science* **2001**, *294*, 1317-1320.

(29) Postma, H. W. C.; Teepen, T.; Yao, Z.; Grifoni, M.; Dekker, C. *Science* **2001**, *293*, 76-79.

(30) Yao, Z.; Dekker, C.; Avouris, P. *Carbon Nanotubes* Springer: New York,

2001; Vol. 80, pp 147-171.

(31) Duan, X. F.; Huang, Y.; Lieber, C. M. *Nano. Lett.* **2002**, *2*, 487-490.

(32) Ouyang, M.; Huang, J. L.; Lieber, C. M. *Acc. Chem. Res.* **2002**, *35*, 1018-1025.

(33) Ouyang, M.; Huang, J. L.; Cheung, C. L.; Lieber, C. M. *Science* **2001**, *291*, 97-100.

(34) Rueckes, T.; Kim, K.; Joselevich, E.; Tseng, G. Y.; Cheung, C. L.; Lieber, C. M. *Science* **2000**, *289*, 94-97.

(35) Kong, J.; Franklin, N. R.; Zhou, C. W.; Chapline, M. G.; Peng, S.; Cho, K. J.; Dai, H. J. *Science* **2000**, *287*, 622-625.

(36) Kong, J.; Chapline, M. G.; Dai, H. J. *Adv. Mater.* **2001**, *13*, 1384-1386.

(37) Hafner, J. H.; Cheung, C. L.; Lieber, C. M. *Nature* **1999**, *398*, 761-762.

(38) Dai, H. J.; Hafner, J. H.; Rinzler, A. G.; Colbert, D. T.; Smalley, R. E. *Nature* **1996**, *384*, 147-150.

(39) Kymakis, E.; Amaratunga, G. A. J. *Appl. Phys. Lett.* **2002**, *80*, 112-114.

(40) Kymakis, E.; Alexandrou, I.; Amaratunga, G. A. J. *J. Appl. Phys.* **2003**, *93*, 1764-1768.

(41) Kymakis, E.; Amaratunga, G. A. J. *Synthetic Met.* **2004**, *142*, 161-167.

(42) Banerjee, S.; Wong, S. S. *Nano Lett.* **2002**, *2*, 49-53.

(43) Banerjee, S.; Wong, S. S. *J. Am. Chem. Soc.* **2002**, *124*, 8940-8948.

(44) Haremza, J. M.; Hahn, M. A.; Krauss, T. D. *Nano Lett.* **2002**, *2*, 1253-1258.

(45) Banerjee, S.; Wong, S. S. *Nano Lett.* **2002**; *2*; 195-200.

(46) Azamian, B. R.; Coleman, K. S.; Davis, J. J.; Hanson, N.; Green, M. L. H. *Chem. Commun.* **2002**, 366-367.

(47) Baker, S. E.; Cai, W.; Lasseter, T. L.; Weidkamp, K. P.; Hamers, R. J. *Nano Lett.* **2002**, *2*, 1413-1417.

(48) Dwyer, C.; Guthold, M.; Falvo, M.; Washburn, S.; Superfine, R.; Erie, D. *Nanotechnology* **2002**, *13*, 601-604.

(49) Shim, M.; Kam, N. W. S.; Chen, R. J.; Li, Y.; Dai, H. *Nano Lett.* **2002**, *2*, 285-288.

(50) Pompeo, F.; Resasco, D. E. *Nano Lett.* **2002**, *2*, 369-373.

(51) Pantarotto, D.; Partidos, C. D.; Graff, R.; Hoebeke, J.; Briand, J.-P.; Prato, M.; Bianco, A. *J. Am. Chem. Soc.* **2003**, *125*, 6160-6164.

(52) Sun, Y.-P.; Huang, W.; Lin, Y.; Fu, K.; Kitaygorodskiy, A.; Riddle, L. A.; Yu, Y. J.; Carroll, D. L. *Chem. Mater.* **2001**, *13*, 2864-2869.

(53) Sun, Y. P.; Fu, K. F.; Lin, Y.; Huang, W. J. *Acc. Chem. Res.* **2002**, *35*, 1096-1104.

(54) Mickelson, E. T.; Huffman, C. B.; Rinzler, A. G.; Smalley, R. E.; Hauge, R. H.; Margrave, J. L. *Chem. Phys. Lett.* **1998**, *296*, 188-194.

(55) Georgakilas, V.; Kordatos, K.; Prato, M.; Guldi, D. M.; Holzinger, M.; Hirsch, A. *J. Am. Chem. Soc.* **2002**, *124*, 760-761.

(56) Georgakilas, V.; Tagmatarchis, N.; Pantarotto, D.; Bianco, A.; Briand, J. P.; Prato, M. *Chem. Commun.* **2002**, 3050-3051.

(57) Bahr, J. L.; Yang, J. P.; Kosynkin, D. V.; Bronikowski, M. J.; Smalley, R. E.; Tour, J. M. *J. Am. Chem. Soc.* **2001**, *123*, 6536-6542.

(58) Coleman, K. S.; Bailey, S. R.; Fogden, S.; Green, M. L. H. *J. Am. Chem. Soc.* **2003**, *125*, 8722-8723.

(59) Holzinger, M.; Vostrowsky, O.; Hirsch, A.; Hennrich, F.; Kappes, M.; Weiss, R.; Jellen, F. *Angew. Chem. Int. Edit.* **2001**, *40*, 4002-4005.

(60) Banerjee, S.; Wong, S. S. *J. Am. Chem. Soc.* **2004**; *126*; 2073-2081.

(61) An, L.; Fu, Q.; Lu, C.; Liu, J.; *J. Am. Chem. Soc.* **2004**; *126*; 10520-10521.

(62) Tang, Z.; Xu, H. *Macromolecules* **1999**, *32*, 2569-2576.

(63) Curran, S. A.; Ajayan, P. M.; Blau, W. J.; Carroll, D. L.; Coleman, J. N.; Dalton, A. B.; Davey, A. P.; Drury, A.; McCarthy, B.; Maier, S.; Strevens, A. *Adv. Mater.* **1998**, *10*, 1091-1093.